Czech Technical University in Prague

Faculty of Civil Engineering

Department of Mechanics

Mechanical and numerical analyses of titanium trabecular structures of dental implants formed by 3D printing

Mechanické a numerické analýzy titanových trabekulárních struktur dentálních implantátů tvořených 3D tiskem

Master thesis

Master degree study program: Civil Engineering

Field of study: Structural and Transportation Engineering

Supervisor: Ing. Aleš Jíra, Ph.D.

Luboš Řehounek

Prague 2016

ČESKÉ VYSOKÉ UČENÍ TECHNICKÉ V PRAZE
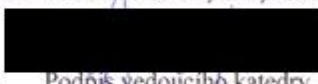
Fakulta stavební

Thákurova 7, 166 29 Praha 6

ZADÁNÍ DIPLOMOVÉ PRÁCE

I. OSOBNÍ A STUDIJNÍ ÚDAJE

Příjmení: Řehounek   Jméno: Luboš   Osobní číslo: 395967

Zadávající katedra: Katedra mechaniky

Studijní program: Stavební inženýrství

Studijní obor: Konstrukce a dopravní stavby

II. ÚDAJE K DIPLOMOVÉ PRÁCI

Název diplomové práce: Mechanické a numerické analýzy titanových trabekulárních struktur dentálních implantátů tvořených 3D tiskem

Název diplomové práce anglicky: Mechanical and numerical analyses of titanium trabecular structures of dental implants formed by 3D printing

Pokyny pro vypracování:

Popis základních principů v oblasti implantologie, vývoj materiálů a technologie jejich vyrábění. Charakteristika trabekulární struktury, její pozice a využití v dentální implantologii. Provedení a vyhodnocení mikromechanických a makromechanických zkoušek trabekulární struktury. Zhotovení numerického modelu 3D struktury a její analýza pomocí MKP.

Seznam doporučené literatury:

Jméno vedoucího diplomové práce: ing. Aleš Jíra, Ph.D.

Datum zadání diplomové práce: 14.10.2016   Termín odevzdání diplomové práce: 8.1.2017

Údaj uveďte v souladu s datem v časovém plánu příslušného ak. roku

▮▮▮▮▮▮   ▮▮▮▮▮▮

Podpis vedoucího práce   Podpis vedoucího katedry

III. PŘEVZETÍ ZADÁNÍ

Beru na vědomí, že jsem povinen vypracovat diplomovou práci samostatně, bez cizí pomoci, s výjimkou poskytnutých konzultací. Seznam použité literatury, jiných pramenů a jmen konzultantů je nutné uvést v diplomové práci a při citování postupovat v souladu s metodickou příručkou ČVUT „Jak psát vysokoškolské závěrečné práce" a metodickým pokynem ČVUT „O dodržování etických principů při přípravě vysokoškolských závěrečných prací".

17.10. 2016   ▮▮▮▮▮▮

Datum převzetí zadání   Podpis studenta(ky)

Abstract

The main focus of this thesis is to investigate and describe a novel biomaterial structure that does not have any previously documented history of testing. The trabecular structure is not yet commercially available for prostheses or implants but seems to be very promising in various aspects such as biocompatibility and mechanical properties. Since this morphologically complex structure cannot be machined, 3D printing was used to create a variety of test specimens. These specimens were then tested by nanoindentation and tensile and compression tests. On the basis of the mechanical tests, a numerical model was created and curve-fitted to represent the mechanical behavior of the trabecular structure. Since future effort will be directed towards utilizing the structure in dental implants specifically, an overview of recent and historic implant materials and methods is presented to point out the benefits of development of new materials and structures. A closer attention is given to implant alloys, titanium implants, material properties and surface treatment. It is expected that further effort beyond the limits of this thesis will be needed to fully describe the complex behavior of the trabecular structure as no comparison with other authors is available yet.

Keywords

Trabecular, Titanium, Dental Implant, Numerical Model, 3D Printing.

Abstrakt

Hlavním cílem této diplomové práce je prozkoumat a popsat chování nové biomateriálové struktury, která doposud nemá žádné zdokumentované materiálové testy. Trabekulární struktura je zatím komerčně nedostupná pro účely protéz či implantátů, ale její potenciální výhody z hlediska biokompatibility či mechanických vlastností se zdají být velmi příznivé. Protože tato morfologicky komplexní struktura nemohla být vyrobena konvenčními metodami obrábění, bylo u její výroby přistoupeno k technologii 3D tisku. Vyrobené vzorky byly následně testovány metodou nanoindentace a tlakovými a tahovými zkouškami. Na základě těchto mechanických zkoušek byl následně vytvořen numerický model, který byl metodou curve-fitting upraven tak, aby reprezentoval mechanické chování trabekulární struktury. Protože budoucí výzkum bude věnován využití struktury v dentálních implantátech, je v práci zahrnut přehed rozličných materiálů a současných i historických metod implantace pro lepší nastínění problematiky a zdůraznění významu vývoje nových materiálů a struktur. Bližší pozornost je věnována zejména implantačním slitinám, titanovým implantátům, mechanickým vlastnostem a povrchovým úpravám. Je předpokládáno, že pro kompletní a spolehlivý popis chování trabekulární struktury bude dále proveden obsáhlejší výzkum, jelikož zatím není možné dosažené výsledky porovnat s ostatními autory.

Klíčová slova

Trabekulární, titan, dentální implantát, numerický model, 3D tisk.

Conflict of Interest Statement

As the author of this master thesis, I declare no conflict of interest. I claim to have written this master thesis solely myself, provided with professional consultations from my supervisor Ing. Aleš Jíra, Ph.D.

I also declare that all literature and materials used in the writing of this master thesis are properly cited in the References chapter.

In Prague, 7. 1. 2016   .███████████████.
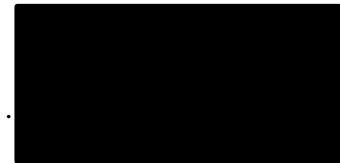
Luboš Řehounek

Acknowledgment

I would like to extend gratitude towards my supervisor Ing. Aleš Jíra, Ph.D. for providing me with professional consultations, information on implants and also practical advice with regard to numerical modeling and writing my thesis. Also, I would like to thank Ing. arch. et Ing. František Denk, Ph.D. for providing me with useful information during our consultations about the geometry of the model and numerical modeling in general. The assistance is greatly appreciated. I would also like to thank Ing. Ivan Laszlo for providing me with an online consultation on the failure of the model and other computation problems.

Table of Contents

1 Introduction

The word „implant" can have multiple meanings and can be quite ambiguous in the conception of contemporary society. To accurately address the subject of this thesis, I consider its definition very important. The description I find to be best fitting for my specific issue is as follows: „An implant is an artificial material or tissue that shows biocompatibility upon its surgical implantation". This is a definition introduced by the International Journal of Oral and Maxillofacial Implants (JOMI). In other words, an implant represents an extrinsic material the body of the patient is able and willing to accept and fully integrate.

The general purpose of most implants is to substitute or enhance the original living tissue of the patient in some way, shape or form. From now on, whenever I will address the word „implant", I will therefore mean the living or artificial replacement tissue introduced in the body of the patient in order to compensate for the loss, extraction or deterioration of the original tissue. Implants are man-made devices, contrary to transplants, which are living tissues transferred from a healthy specimen into the body of the patient.

There are multiple reasons as to why should one want an implant introduced in their body. Throughout the years of human evolution, mankind has used implants of various shapes, materials and purposes to fill in the role of damaged tissue [1]. Materials like ligature wire made of gold, stone, oxen bones, ivory or animal shells were used to substitute missing teeth since the dawn of ancient civilizations [2]. The history of dental implants goes as far back as 3000 B.C. [3], the period of ancient Egyptians.

I have chosen to cover this topic because with the advanced technology and manufacturing process we have at our disposal today, the whole idea of implants is growing rapidly and implants become more and more available. Whereas before only people of privileged position could afford to undergo this kind of treatment, now it is a widely available and also suggested option for nearly everybody who suffers from damage related to their bone tissue. I would like to present a comparison to confirm this fact. In the year 2008, searching the term „implant" in the PubMed database netted a total of 46,575 papers, with 9,768 of them being identified to the term „dental implant" (21%) [3]. Now, at the time of writing this thesis in 2016, the same search extracted 97,655 papers when searching

„implant" and 37,185 papers for „dental implant" (38%). The total value has been doubled and the number of papers specifically written on dental implants has been quadrupled. This simple comparison shows us how much have implants (dental implants in particular) gained in popularity and attention over the course of mere 8 years.

There is, however, still a great many number of unanswered questions and challenging problems with regard to this issue. One of them is the main motivation behind creating the trabecular structure – the difference of material properties at the interface of individual dental materials. Dental implants have advanced tremendously, evolving from primitive hammered-down pieces of bone into fine, precisely shaped metal products. Yet, they still have one bad common denominator, and that is the interconnection between the implant and the bone. Trabecular structure is there as a future prospect and a potential solution to the problem of both the bad interconnection and material difference at the interface of materials. If proven to be satisfying in medical, mechanical and economic regards, trabecular structure could be the future of dental implants, improving upon the former variants.
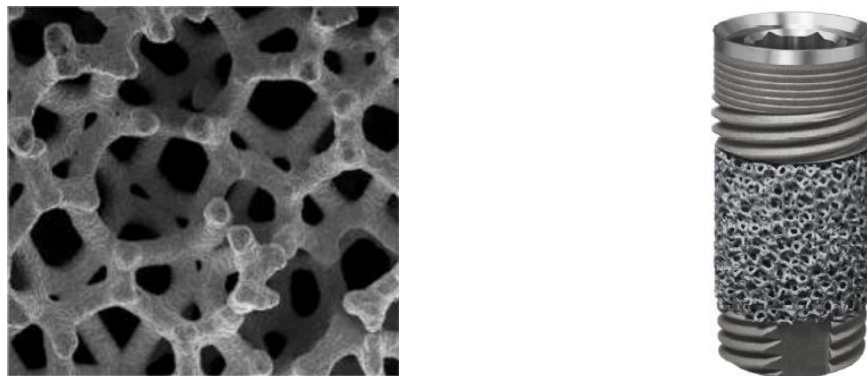

Fig. 1: Illustration of a porous tantalum trabecular metal (PTTM) – microstructure (left) and the overall structure of a titanium PTTM-enhanced dental implant (right) [4].

The methods used to experimentally analyze the properties of the structure, mainly Young's modulus E and reduced modulus E_r, are micromechanical and macromechanical tests, specifically nanoindentation and global tensile and compression tests. The mechanical tests have been conducted as a pilot experiment and cannot be therefore compared with results published by any other author.

The complete mechanical analysis of the trabecular structure calls out for a numerical model. The nature of deformation of the structure is yet unknown, making the development

of any model without experimental data very challenging. However, with the data provided by micromechanical and macromechanical tests, it is possible to develop a numerical model including the nonlinear behavior required to describe the stress-strain diagrams obtained during the mechanical tests. This data served as a baseline for curve-fitting, a necessary process in the creation of the numerical model based on experimental data. The manipulation of the properties of the model has been done in order to fit in the two most important regions – the yield strength and ultimate strength and their respective values of corresponding elongation.

2 Brief overview of alternative methods of treatment

The approach of treatment has multiple options. Before we further delve into the topic of dental implants specifically, let us briefly address other options of treatment as well. There are generally three basic solutions to the problem of treating missing teeth in the jaw – dentures, bridgework and implants.

2.1 Dentures

The first option of treatment is denture. A denture, sometimes referred to as false teeth, is a removable replacement for missing teeth and tissues surrounding them. According to the number of teeth missing, they are either complete or partial (Fig. 2). Dentures can also be divided into another two major groups – conventional and immediate [5]. A conventional denture is ready for placement approximately 8 to 12 weeks after the teeth have been removed. Immediate dentures are made in advance and are ready for placement immediately after the extraction. They bring the benefit of replacing the teeth immediately, allowing the patient an undisrupted period of time during the healing process. However, as the bone remodels itself and the gums shrink, adjustments to the immediate denture are necessary in order to remain functional. Conventional dentures should always be considered as the definitive answer, replacing immediate dentures after the healing process [5].

Fig. 2: Images of different types of dentures. A partial denture (left) and a complete denture (right) [6].

Dentures are usually removable and provide the necessary masticatory and esthetic functions. However, they are generally considered as an obsolete method of treatment [7], simply because they cannot fully substitute the original teeth and are not nearly as stable as a dental implant. This fact is preventing the patient from performing everyday actions with the comfort of a dental implant or the original tooth.

2.2 Bridgework

The second option at our disposal is bridgework. There are generally three main types of bridgework [8]. The first and most common type is a traditional bridge. The treatment procedure using a traditional bridge can be seen in Fig. 3. The downside of this method is that teeth placed adjacent to the missing tooth have to be prepared (sized down) so the crowns on both sides can fit onto them. When everything is prepared, the crowns are cemented onto the adjacent filed teeth and the bridge is complete. Traditional bridges can provide the patient with a stable foundation to perform everyday activities – mastication, smiling, speaking etc. They also help keep other teeth in place since they fill the empty space between adjacent teeth, making the drifting impossible or keeping it at its minimum [8] and are also esthetically pleasing [9]. However, traditional bridges still do not provide any load to the bone underneath the missing tooth (as there is no contact since the site is bridged), which can lead to bone loss. This is a fact that makes dental implants superior to them, as they can provide the necessary load to maintain the bone mass.

Fig. 3: A step-by-step illustration of applying a bridgework [11].

The second type of bridge is the cantilever bridge. While they are still being used, they have been on the decline as research has proven that they are not a very suitable solution to the problem as they suffer from mechanical and technical difficulties [12]. Due to the mechanical nature of the cantilever, they sometimes behave like a lever, prying the abutment out from the healthy tooth and causing a loss of retention. There can either be one or multiple abutment teeth.

The third type of bridge is the Maryland bridge (resin-bonded bridge). The main distinguishing part of this bridge is a metal or porcelain framework that holds the false tooth and bonds it to the adjacent tooth or teeth by resin. The advantage of the Maryland bridge is that the adjacent teeth do not need to have their enamel sanded away. A potential disadvantage might be the strength of the resin that binds the framework to the adjacent teeth, especially in areas where the masticatory stresses are very high, like the molars [13]. Another potential disadvantage is the discomfort of the framework getting in the way of one's gums or bite [13]. This is yet another disadvantage of the bridgework that does not concern dental implants.

Fig. 4: Imagery of different types of dental bridges. A cantilever bridge (left) [14], and a resin-bonded (Maryland) bridge (right) [15].

3 Implantology

3.1 History of dental implants

The history of dental implants is very rich and fascinating, revealing mankind's resourcefulness, creativity and ability to use contemporary technology and materials. One of the most famous and documented archaeological findings of dental implants stretches back to the Mayan civilization at around the year 600 AD [16], [17]. In 1931, archaeologists found remains of the body of a young (approximately 20 years old) Mayan woman in the area where Honduras is today. Her lower jaw had three tooth-shaped pieces of shells placed in it to substitute for her missing incisor teeth [16], [17], [18]. It has been stated that these shell implants were indeed functional and were placed in the body of the woman during her life, contrary to the belief that they only served as post-mortem, esthetic accessories [18]. But the history goes back even further. As long ago as 2500 BC, the ancient Egyptians used golden ligature wire to stabilize loose teeth involved in periodontal issues [2]. It is even documented in their manuscripts that this method of treatment often caused severe toothaches. It is also believed that Egyptians used shells just as the Mayans did [19]. Various materials such as bone, shells or stone were used in order to preserve the looks and functions of the ancient human's dentition.

Fig. 5: Various types of ancient dental restorations. Ligature wire and staples on the left [20], animal shells and bones on the right [21].

In the Middle Ages, implantation revolved mostly around allografts and xenografts [22], [23]. An allograft is a transplant of an organ or a tissue from a donor of the same species with a different genotype. A xenograft is also a transplant, but it is grafted from an individual of completely different or unlikely species (for example a tissue from a baboon transplanted to a human) [24]. It was very common that the transplants came from dead people or livestock. During the time between 1500's and 1800's, teeth in Europe were collected from cadavers or from underprivileged commoners to be used as allotransplants [2]. This practice, however, did not have much success as it was often the cause of severe inflammation or even death [23].

Another evolution of implants happened at the end of the 1800's in USA, where specialists were able to implant false teeth lasting as long as 8 to 11 years [23]. A wide array of materials was already available at that time, including gold, platinum, rubber, wood, tin or lead.

In late 1930's, another great invention was introduced by Drs. Alvin and Moses Strock, who experimented with Vitallium, a chromium-cobalt-molybdenum alloy. They observed the effect of screws made from this material that were placed in hipbones of patients by other physicians and decided to implant them in humans and dogs in order to provide the anchorage for the replacement teeth. For this invention, they have been later acknowledged in selection of a biocompatible material usable in human dentition [25].

Fig. 6: A crownless Vitallium implant replacing a human tooth by Strock brothers [26].

In the 1940's, implants took another turn for the better as Swedish physician Dahl developed a subperiosteal (placed above the bone) implant [25] with flat abutments and screws which lay over the crest of the alveolar ridge [2]. His work has been continued by Goldberg and Gershkoff in USA to produce a cobalt-chromium molybdenum implant with

an extension including the external oblique ridge [27]. This concept was further investigated by Lew, Bausch and Berman in 1950 [28] and improved upon. The whole process was being streamlined and the placement of screws and the shape of the framework optimized.
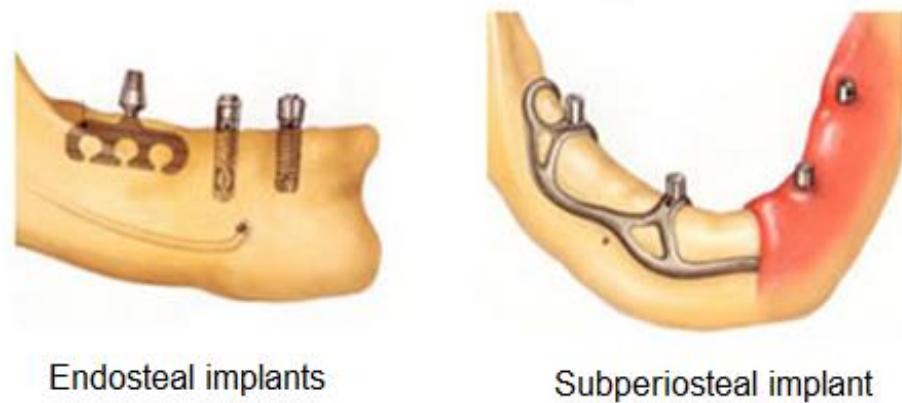

Fig. 7: Position of the implant in regard to the jawbone – endosteal (inside the bone) implants on the left and subperiosteal (on the surface of the bone) on the right [29].

The greatest milestone in the evolution of dental implants happened just a few years later. In 1952, Swedish orthopaedic surgeon Per-Ingvar Brånemark observed the process of bone healing response and regeneration. To perform this experiment in vivo, he adapted an experimental chamber developed at the Cambridge university called the "rabbit ear chamber" [18], [22]. This chamber was used to observe the functioning of bone marrow of rabbits in vivo. At that time, he was unable to obtain the original material, tantalum, so he used titanium instead. He performed a series of long investigations and when he finally wanted to retrieve the chamber and reuse it, he found to his discontent that it could not be removed from the bone [30].

Brånemark did not put much weight onto this discovery until the 1960's when he accepted professorship in the Department of Anatomy at Gothenburg University. Then, he started investigating more and used a titanium lens casting to observe the structure and workings of blood cells in human arms under numerous conditions, such as cigarette smoking. This research brought a great deal of information on the behavior of the blood cells but also ultimately proved that titanium is very compatible with human tissue as it did not provoke any immunological reactions. It was after this experiment that Brånemark gave titanium a brand new purpose as he began devising plans of introducing titanium in the

medical field [22]. Although at first he thought that his main work should be dedicated to knee and hip surgery, later on he finally decided that the jaw is far more accessible to continuous observations and also provides many specimens to work with as edentulism (loss of all teeth in one or both jaws) is very widespread throughout the population [18].

During the following years, Brånemark and his team focused mainly on the effects of titanium screws in living organisms and the biological responses associated with implantation. With these screws, they made various experiments on dogs, observing the conditions of bonding and the overall response to the extrinsic material [22]. As the understanding deepened and the field of their studies began to be more and more important, Brånemark felt the need to address the process of bonding the metal with bone. The term he chose was osseointegration, from the Latin words os (bone) and integro (to renew). This is a term that is now used very frequently and is also one of the keypoints behind creating new structures, such as the trabecular structure. He and his team then proceeded to create numerous papers and carry out a vast volume of research and experiments towards the creation of titanium dental implants [31].
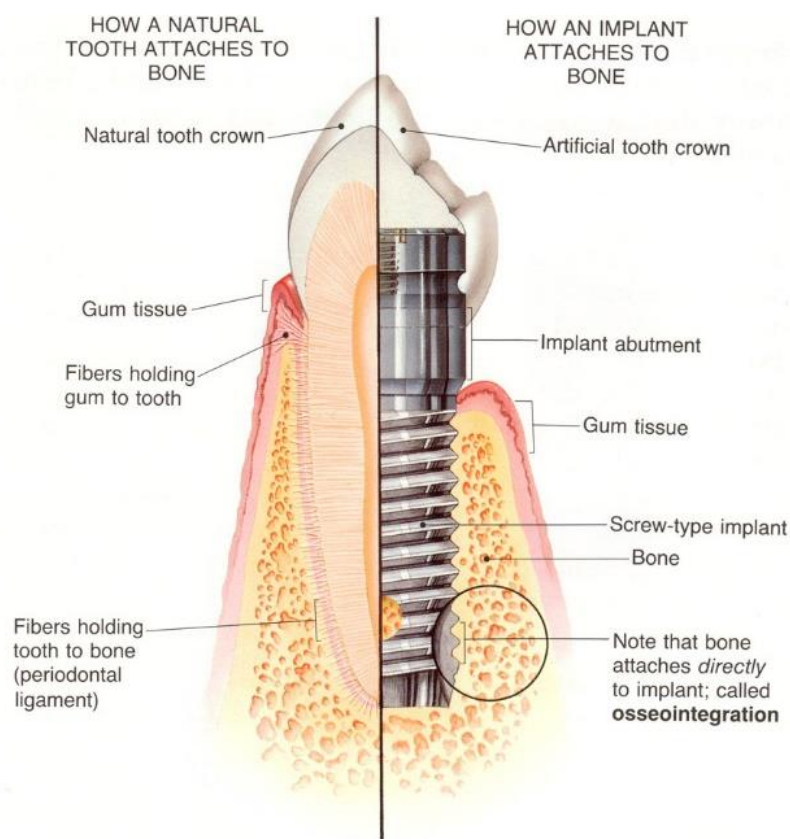

Fig. 8: Image of a section showing the difference in the contact region of a natural tooth and an osseointegrated implant [32].

In 1965, Brånemark successfully implanted the first titanium implant [33]. His patient, Gösta Larsson was the first person to ever receive a titanium dental implant and it changed his life tremendously. Brånemark placed four titanium screw implants into the man's mandible, waited several months and then proceeded to place a set of false teeth. All of the titanium fixtures survived and the patient's life had been changed for the better [28].

This method proved to be very effective. Eventually, in 1975 Brånemark won the approval of the team of three independent Swedish dentists who reported to the Swedish National Health and Welfare Board. As the result of this event, the Brånemark method became fully covered by the Swedish national health insurance system in 1976. A year later, in 1977, Brånemark began to train the first Swedish dental experts in his methods and techniques [28].

The evolution of dental implants went on and many other improvements followed. In 1978, Brånemark entered into a commercial partnership with Bofors AB. With this company as the parent company, Nobelpharma AB (later renamed Nobel Biocare) was founded in 1981 [18]. In 1997, the first tapered implant (Fig. 9 left) was created and in 1998 the All-on-4 system was invented (Fig. 9 right). This groundbreaking method of implantation dramatically changed the lives of patients who have been previously unable to have dental implants placed in their jaw due to bone loss [33].

Fig. 9: Left – tapered implants [34]; right- the All-on-4 system, where a whole arch of artificial crowns is supported only by 4 dental implants [35].

During the 80's, the word spread to the U.S. as George Zarb from the Toronto University, who was trained under Brånemark, organized the 1982 Toronto conference on Osseointegration in Clinical Dentistry. More than 70 universities responded and sent their representatives. At this important conference, Brånemark presented more than 15 years of his diligent research on humans and animals [28].

Up to 2014, more than 7 million Brånemark system implants have been placed [18] and hundreds of companies already produce dental implants. The demand for dental implants is very high, as approximately 450,000 implants are placed every year. In the case of single tooth replacement, the expectation of success rate is around 95 % [31].

3.2 Approaching treatment

The purpose of dental implants is to provide a stable, non-moving anchor in the jawbone. This anchor serves as a support for the artificial replacement tooth (crown), which is installed on the top of the dental implant (Fig. 10). The whole extrinsic body then comprises of the dental implant, crown and the abutment, which is an interconnecting piece of metal installed on top of the dental implant. Treatment in the form of dental implants should be considered as a viable option for the replacement of missing or damaged teeth as it provides more predictable results than bridgework, resin-bonded bridges or endodontic treatment [36] and also does not cause bone loss [19]. Dental implants therefore have a way of keeping the jawbone healthy and functional and are also fulfilling the esthetic demands.

Fig. 10: Conventional implant and its parts (left) and its placement in the jaw (right) [37].

It is very important to acknowledge the need of treatment as fast as possible. The earlier a patient recognizes the problem, the better and more successful can the procedure of treatment be. According to Wolff's law, *The Law of Bone Remodeling*, presented more than a hundred years ago, the bone of a healthy specimen will always adapt to the conditions of the load [38]. Therefore, if the tooth has been extracted or damaged and is no longer providing sufficient load to the bone underneath it, the bone will start to remodel itself. As a result, the bone will become weaker and less dense, as it no longer needs to withstand the previously provided load. The fact that dental implants provide such load makes them significantly superior to other methods of treatment.

The procedure of implantation is usually done in three sittings and is as follows – during the first sitting, the dental surgeon makes a small incision in the gingiva where the implant will be placed. After that, they drill a hole in the patient's jawbone and clean it up for the placement of the implant. After the implant is placed, the hole in the gingiva is stitched together and the patient now enters the healing phase, during which the bone surrounding the implant heals and bonds with the metal (a process previously described as osseointegration) [39]. After this healing period, which is usually three to five months long, the patient visits the surgeon again. During the second procedure, the wound is opened again, exposing the implant. A healing cap is screwed on the top of the implant in order to shape and heal the gingiva. During the third sitting, the healing cap is removed and the abutment is screwed into the implant, followed by placement of the crown. Multiple variations of this procedure are also possible, resulting in either two-stage, or even one-stage procedures [39].

3.3 Types of implants

Historically, there are four main types of dental implants that have been used in clinical dentistry. They include the subperiosteal (Fig. 11 A), blade (Fig. 11 B), ramus frame (Fig. 11 C) and endosseus screw or cylinder-shaped implants (Fig. 11 D) [31]. However, since most of contemporary surgeons use endosseous implants, other types will only be illustrated briefly and the main attention will be directed towards endosseous implants.
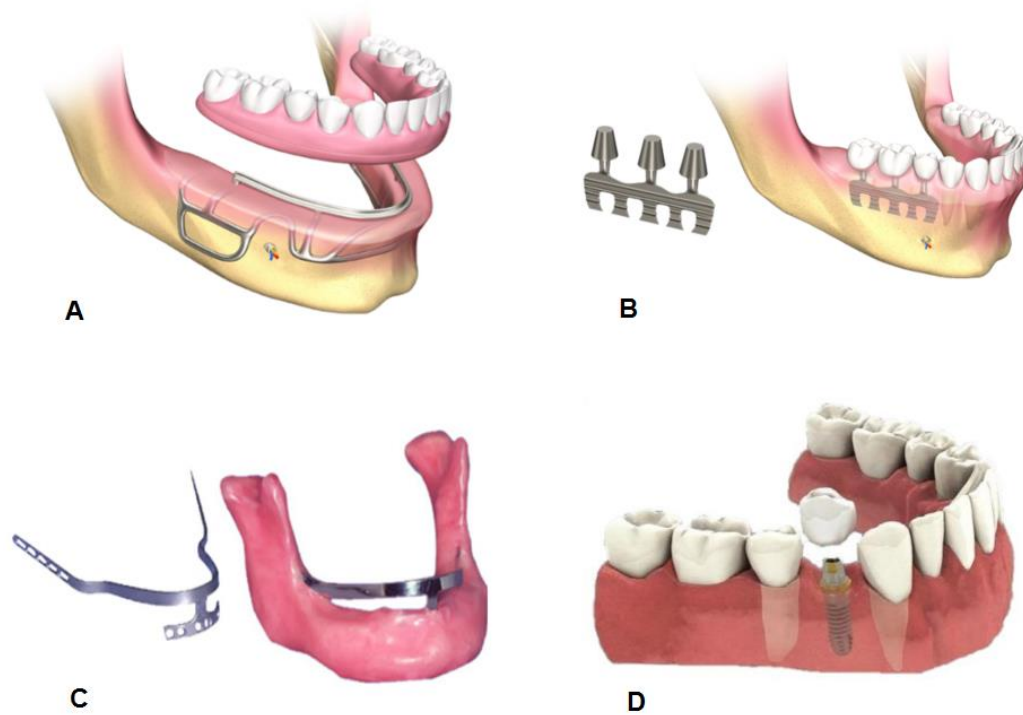
Fig. 11: Different types of implants based on their shape and position towards the jawbone. A) subperiosteal implant [40], B) blade implant [40], C) ramus frame implant [41], D) endosseous implant [42].

Endosseous dental implants are available in different shapes, diameters, sizes, lengths, surface modifications, coatings, materials and other properties. Nowadays, dental surgeons have to choose from thousands of implant types with different properties and attributes [43].

According to the method of placement, endosseous implants can be divided into 2 major subgroups – screw-threaded implants and push-in implants. The push-in implants are coated twith a layer of osseointegrative layer and simply pushed into the drilled, cleaned hole and left to osseointegrate. Screw-threaded implants are placed onto the top of the drilled hole and screwed down.

Fig. 12: Variants of coated push-in implants (left) and screw-threaded implants (right).

4 Implant alloys and biocompatibility

Nowadays there are generally 2 major groups of materials used in implant dentistry – metals (mainly titanium and its alloys) and ceramics. A great many other materials have been used in the past – materials like gold, stainless steel, cobalt-chromium alloys, various resins and many more. Most of these materials, however, did not meet the necessary requirements for longevity, biocompatibility and mechanical properties and their production ceased as new, better materials arose [44].

4.1 Bioceramics

Bioceramics is a rather new material in implant dentistry. It has been introduced in the 1990's as a viable alternative to titanium alloys [44]. Most ceramic implants are zirconia implants. Ceramics have one substantial benefit over titanium – their color. If the gums are worn out, the dark, grayish surface of titanium can be visible through the peri-implant gingiva, impairing the overall esthetics (Fig. 13 left). Ceramic implants are white and their esthetics are more appealing in this manner. Another great benefits are thermal non-conductivity, no piezo-electric currents between different metals in the mouth and no corrosion [46].

Fig. 13: Comparison of a titanium-treated case (left) with receding gums and bioceramics (right). The grayish surface of titanium might appear unesthetic compared to bioceramics, where no defects are visible as the implant is white [45].

Zirconia implants, however, do not provide much documented history of success as they have not been around for a long period of time. They are also known to be prone to shear and tensile loading. Surface wear may then lead to premature failure of the implant. Ceramics also have poor bonding abilities, making osseointegration questionable [47]. Surface modifications of ceramic dental implants are therefore a way of optimizing the bonding process [48]. Micro-roughness modifications (sandblasting, acid-etching), applying bioactive coatings (collagen, calcium phosphate, bisphosponate) and other various modifications are often performed in order to prepare the surface of the implant for osseous healing [49]. A picture of a ceramic implant taken with an optical microscope is shown in Fig. 14.
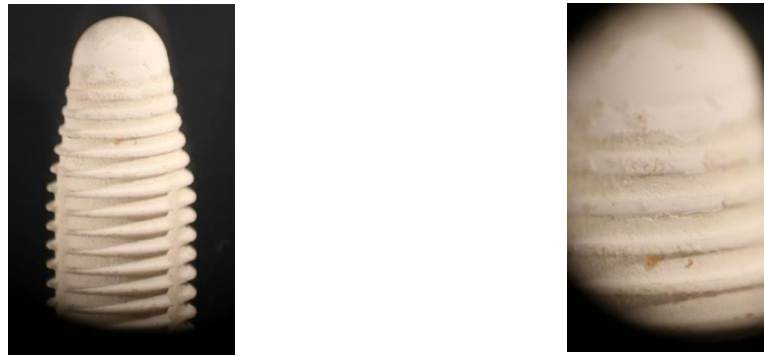
Fig. 14: Images of a bioceramics implant taken with an optical microscope. Overall image of the implant (left) and a magnified image of the upper area (right).

4.2 Titanium alloys

The use of titanium alloys in various areas of biomedical engineering is now a standard gold rule. It is mainly due to their attractive properties – very high tensile strength, corrosion resistance, low density, low Young's modulus (considering relations between the alloy and human bone and tissue) and good ductility. On the other hand, titanium alloys also have one very specific weakness – they are rather expensive, which is a fact that is limiting the potential of their usage as conventional materials. Various efforts have been made to reduce their cost, such as alloying with various elements, thermo-mechanical treatments and different approaches in the production process [50].

To better fit the natural environment of human body, it is desirable to reduce the elastic modulus of titanium alloys, making their mechanical behavior more similar to that of human

bones and tissue [51]. An overview of various titanium and other different alloys is shown in Fig. 15.
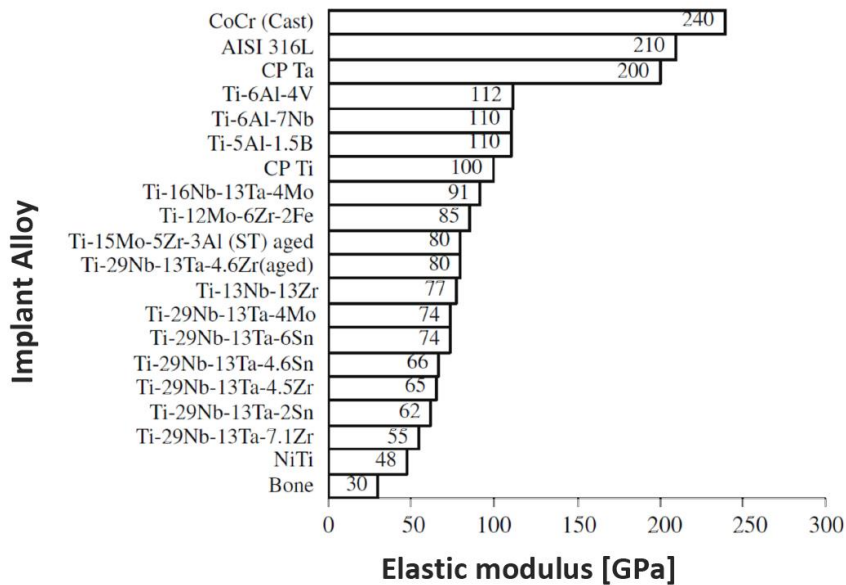

Fig. 15: Moduli of elasticity of various biomedical alloys [52].

Titanium has one great benefit over zirconia implants – it is a well-documented history of success, as they have been used for a longer period of time. Titanium implants can easily reamain functional after 25-30 years of service [46]. Titanium implants are also much more versatile than zirconia implants. Since zirconia is a one-piece system, there is not much space for fine-tuning and rectification of the implant. Unlike zirconia, titanium implants are a two-piece system comprising of the body of the implant, which substitutes the root, and the abutment, onto which the artificial crown is placed. This system allows for a custom position placement of the implant and even slightly off-angle positions with customized, angled abutments, which are sometimes needed in case of local bone loss [46] (Fig. 16).

Fig. 16: Variants of angled abutments for special applications [53].

Titanium is an allotropic material, which means it can exist in multiple crystalline states. There are two of them – the low-temperature α-phase and the high-temperature β-phase. The α-phase has a close-packed hexagonal crystal structure, whereas the β-phase has a body-centered cubic (BCC) structure (Fig. 17) [54]. The transition from the low-temperature α-phase into the high-temperature β-phase occurs at 882°C, thus implying the use of different alloying elements with different mechanical properties. Therefore, using various alloying elements allows for stabilizing titanium in its respective phases.
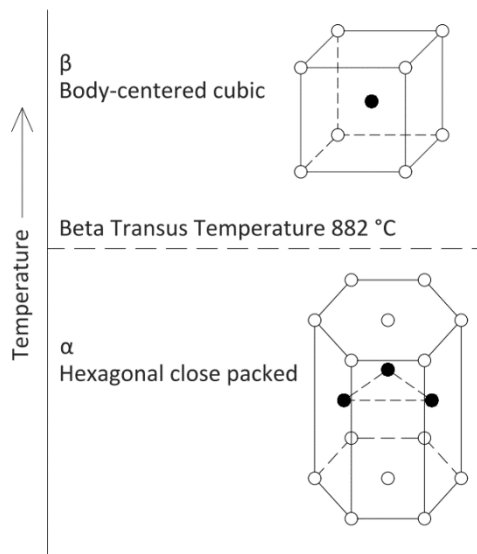
Fig. 17: Two allotropic forms of titanium. The transition from the hexagonal α-phase to the BCC β-phase occurs at 882°C [54][54].

Choosing the elements for a specific alloy is bound with determining the final structure. The choice of the elements comes from their ability to stabilize either the α or β phase. The most common α-stabilizing elements for titanium alloys are aluminum, oxygen, nitrogen, gallium and carbon. Elements used for stabilizing the β-phase can be divided into two sections – elements forming the β-isomorphous-type or the β-eutectoid-type. The isomorphous-type binary system-forming stabilizing elements are molybdenum, vanadium and tantalum, while the eutecoid-type stabilizing elements are copper, manganese, chrome, iron, nickel, cobalt and hydrogen. Zirconium, tin and silicon are considered to be neutral, considering their ability to stabilize either phase [55].

Tab. 1: Critical concentrations (wt.%) of β-stabilizing elements required to retain 100% of the β–phase after quenching in binary Ti alloys [56].

Element	Type	Critical concentration (wt.%)
Molybdenum	Isomorphous	10.0
Niobium	Isomorphous	36.0
Tantalum	Isomorphous	50.0
Vanadium	Isomorphous	15.0
Tungsten	Isomorphous	25.0
Cobalt	Eutectoid	6.0
Copper	Eutectoid	13.0
Chromium	Eutectoid	8.0
Iron	Eutectoid	4.0
Manganese	Eutectoid	6.0
Nickel	Eutectoid	8.0

The defining attribute of β-titanium alloys is their ability to remain 100 % stable when quenched from the β-phase field to room temperature. This stability is provided by alloying titanium with the β-phase stabilizing elements. By providing the alloy with certain elements, we can stabilize either phase of titanium. Various elements can be used to lower the transus temperature required to provide transformation from the α to the β-phase. This temperature is the lowest temperature in which 100% of the β-phase will exist. Other elements can be used to increase the size of the β-phase field or the α-phase field or create a combination of the two [56]. An overview of different α, β and α+β biomedical titanium alloys is shown in Tab. 2.

The Ti-6Al-4V alloy deserves more attention in particular, as it is the commonly used alloy in total hip prostheses, dental implants and other biomedical applications. It is an α+β titanium alloy with an excellent strength to weight ratio and very good corrosion resistance. Aside from the biomedical field, the Ti-6Al-4V alloy plays a huge role in aerospace, automotive, chemical plant, power generation, oil and gas extraction and many other industries [57], where low density, high performance and cost-effectivity demands the use of advanced materials.

Tab. 2: Various dental implant alloys and their mechanical properties [51].

Alloy	Tensile strength [MPa]	Yield strength [MPa]	Elongation [%]	Reduction in area [%]	Modulus [GPa]	Type of alloy
cp Ti grade I	240	170	24	30	102.7	α
cp Ti grade 2	345	275	20	30	102.7	α
cp Ti grade 3	450	380	18	30	103.4	α
cp Ti grade 4	550	485	15	25	104.1	α
Ti-6-Al-4V ELI (mill annealed)	860-965	795-875	10-15	25-47	101-110	α+β
Ti-6-Al-4V (annealed)	895-930	825-869	6-10	20-25	110-114	α+β
Ti-6Al-7Nb	900-1050	880-950	8.1-15	25-45	114	α+β
Ti-5Al-2.5Fe	1020	895	15	35	112	α+β
Ti-5Al-1.5B	925-1080	820-930	15-17	36-45	110	α+β
Ti-15Sn-4Nb-2Ta-0.2Pd						
(Annealed)	860	790	21	64	89	
(Aged)	1109	1020	10	39	103	
Ti-15Zr-4Nb-4Ta-0.2Pd						α+β
(Annealed)	715	693	28	67	94	
(Aged)	919	806	18	72	99	
Ti-13Nb-13Zr (aged)	973-1037	836-908	10-16	27-53	79-84	β
TMZF (Ti-12Mo-6Zr-2Fe) (annealed)	1060-1100	100-1060	18-22	64-73	74-85	β
Ti-15Mo (annealed)	874	544	21	82	78	β
Tiadyne 1610 (aged)	851	736	10		81	β
Ti-15Mo-5Zr-3Al						β
(ST)	852	838	25	48	80	
(aged)	1060-1100	1000-1060	18-22	64-73		
21RX (annealed) (Ti-15Mo-2.8Nb-0.2Si)	979-999	945-987	16-18	60	83	β
Ti-35.3Nb-5.1Ta-7.1Zr	596.7	547.1	19	68	55	β
Ti-29Nb-13Ta-4.6Zr (aged)	911	864	13.2		80	β

Fig. 18: Figures showing geometrically modified Ti-6Al-4V ELI (extra-low interstitial) implants. Geometrical model (left) and cylinder-shaped implants with parallel beams (right).

The Ti-6Al-4V alloy is an α+β alloy with the alpha hexagonal close packed structure and beta body-centered cubic in the microstructure at room temperature Fig. 19 [58]. It is usually manufactured in two variants – the standard Ti-6Al-4V and the Ti-6Al-4V ELI (extra-low interstitial), which is a higher-purity alloy with lower specified limits on Fe, C and O. An overview of the chemical composition of this alloy as well as pure (cp) titanium is shown in Tab. 3.

Tab. 3: Chemical composition of various grades of cp titanium and Ti-6Al-4V alloys [59], [60], [61], [62].

Titanium	N	C	H	Fe	O	Al	V	Ti
cp Ti grade I	0.03	0.10	0.015	0.02	0.18	-	-	balance
cp Ti grade II	0.03	0.10	0.015	0.03	0.25	-	-	balance
cp Ti grade III	0.03	0.10	0.015	0.03	0.35	-	-	balance
cp Ti grade IV	0.03	0.10	0.015	0.05	0.40	-	-	balance
Ti-6Al-4V	0.05	0.08	0.015	0.30	0.20	5.50-6.75	3.50-4.50	balance
Ti-6Al-4V ELI	0.05	0.08	0.012	0.10	0.13	5.50-6.50	3.50-4.50	balance
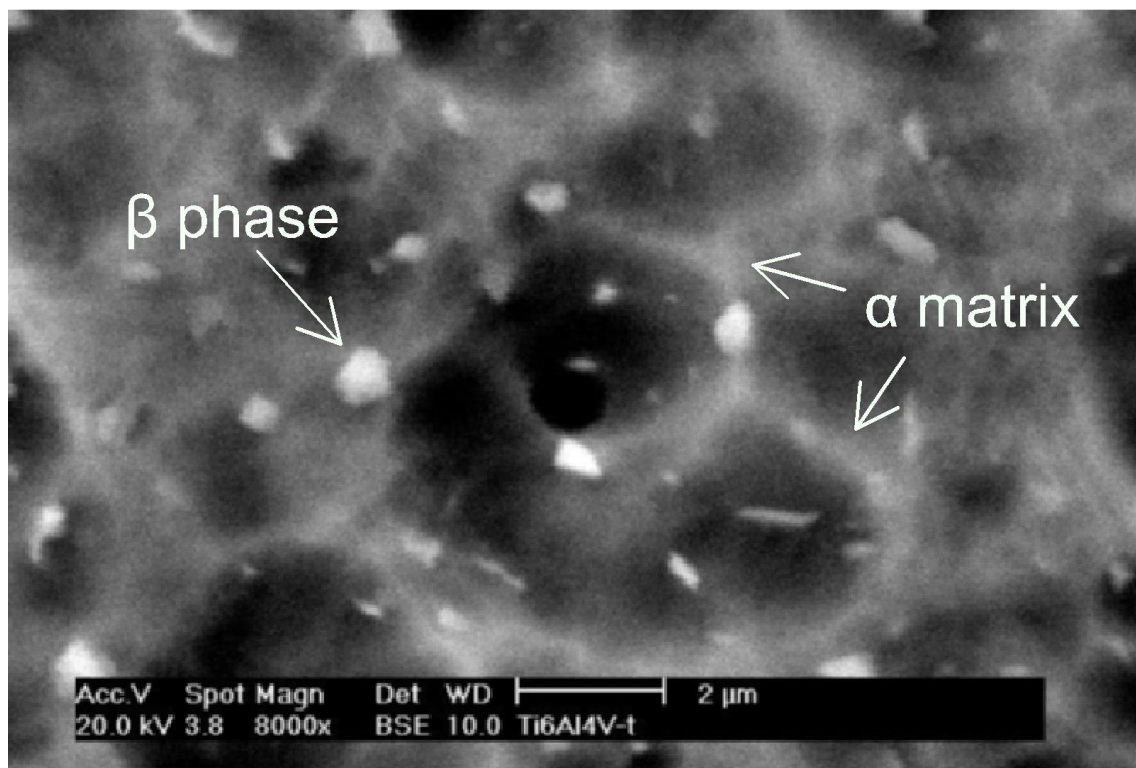
Fig. 19: SEM image of the microstructure of a Ti-6Al-4V sample annealed at 800°C for two hours [58].

4.3 Biocompatibility

For the right functionality and risk-free usability in the human body, dental implants have to be biocompatible. That means that every element used in the final alloy must be corrosion resistant, tissue compatible, vital and elastic [63]. Titanium itself, being the most abundant element in the titanium alloy, meets the requirements of biocompatibility to an excellent extent [64], [65].

Recently, effort has been made to produce alloys free of V and Al as toxicity of V and potential neurological disorder impact of Al has been reported [64], [66], [67], [68], [69]. While Al and V are commonly used in α+β alloys, which are currently the gold standard in implant dentistry, attention has been directed towards β alloys, which commonly use Mo, Zr, Nb and Ta as alloying elements (Tab. 2). This trend also corresponds with osteogenesis – it has been reported, that the amount of new bone formation after a few weeks is the greatest for niobium, then for tantalum and titanium (Fig. 20 a) [70]. Moreover, the results provided by H. Matsuno et al. [70] prove that during the 1-4 week period, the newly formed bone tissue was smoothly attached to the metal implant. During the 2-4 week period, the percentage of bone in contact with the implant has also rapidly increased (Fig. 20 b).

a) The amount of new bone formation after 2 and 4 weeks.

b) The percentage of bone in contact with the implant after 2 and 4 weeks.
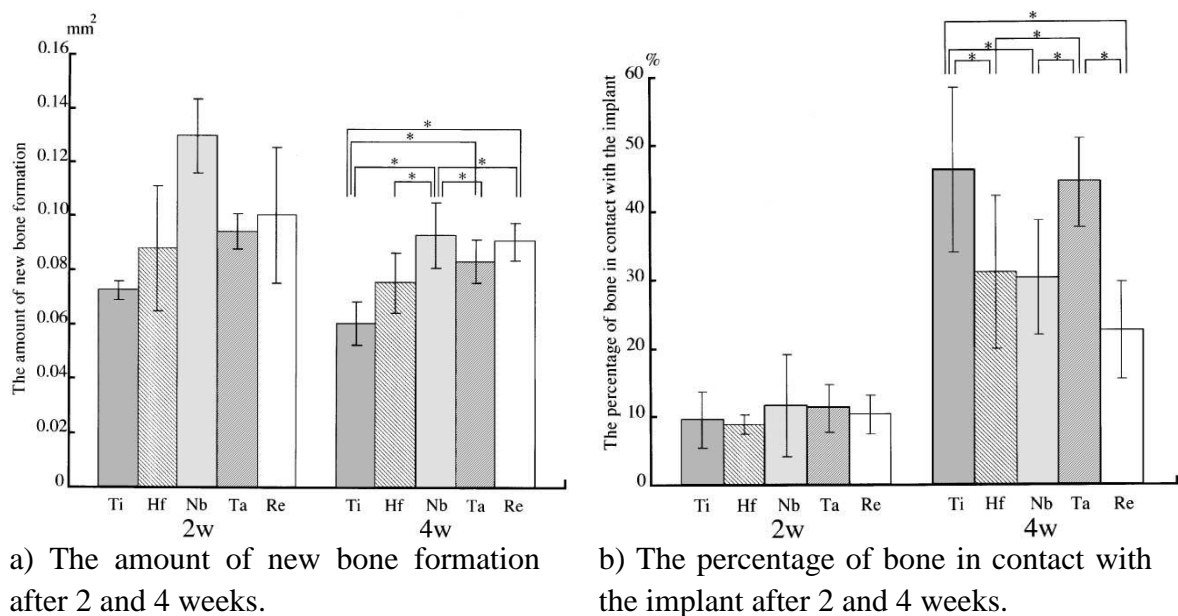
Fig. 20: Two graphs showing the biocompatibility of different alloying elements in regard to new bone formation and bone-implant contact. Vertical lines show standard deviations. *Significant difference ($p < 0.05$) [70].

A series of in vivo tests [63] provides information on the short and long-term biocompatibility of individual materials. According to the reported results, the bonding abilities of tantalum are slightly inferior to those of titanium, with niobium being again the best material. The biocompatibility of niobium can be described as excellent. The results for titanium and tantalum are also very good, making these three metals very suitable for biomedical applications. It should be noted that the experiments were also made for other alloying elements, proving that aluminum is unsuitable for use as a β-stabilizing element due to its limited ability to support cell growth (for conventional implants, it is still successfully used in the form of the α+β Ti-6Al-4V alloy, originally designed for aerospace structures [66]). Zirconium stands as a potentially good biocompatible element, but it has poor corrosion resistance. Molybdenum has very strong β-stabilizing properties on titanium alloys, but it was found that it is moderately toxic, making its use as a biomaterial questionable. Another observable factor considering biocompatibility is cell volume. It has been reported [63] that aluminum, implant steel 316 L and molybdenum exhibit a reduction in cell volume of the specimen, compared to cp-titanium, which has been set as 100% for the sake of comparison. Cell volume of the cells on tantalum and zirconium is not affected, while come cells on niobium show a small increase in volume. Other types of cells do not show any difference in volume or diameter on cp-titanium or niobium. Reduction in cell volume can be considered to be the result of a cytotoxic effect caused by reduction of the cytoplasmatic part of the cell [63].

Commonly used biomedical titanium alloys have (in general) these mechanical properties – tensile strength of 500-1000 MPa, elongation of 10-20 %, modulus of 100-120 GPa for α+β titanium alloys and 55-85 GPa for β-type low-modulus titanium alloys [51]. Low Young's modulus is a welcomed material property as it is desirable to introduce implant material that has similar properties as its predecessor, the organic tissue.

Producing biocompatible alloys suitable for dental implants is also a question of choosing the best alloying elements. While elements like Zr, Nb, Mo and Ta possess very good mechanical properties and biocompatibility, they are also very expensive and have, compared to titanium, very high melting points [71]. With the need for biocompatible implants growing greater and greater due to an increased number of traffic accidents [72] and increasing age of population, the question of sustainable implant production is at hand. While alloys including non-toxic, expensive elements capable of stabilizing the β-phase (such as Nb, Ta, Zr or Mo) represent the superior material, it is also desirable to develop

other, new alloys, including more common, abundant metals [71]. Expensive metals can be substituted with Mn, Fe, Si and Sn, but they are commonly used only as α-stabilizing elements and do not possess the ability to stabilize the β-phase, so at least some addition of the β-stabilizing elements is required [71] and such alloys are the subject of further studies.

The standard α+β alloys contain Al, V or Ni, but they are not to be considered poisonous or strictly health-damaging as their dangerous potential rather lies in long-term implantation effects [71]. These alloys have excellent mechanical properties, very good corrosion resistance and exhibit no immediate biocompatibility issues or rejection in the living tissue environment. Despite the fact they have been used for extensive periods of time, Co-Cr based and Ti-6Al-4V alloys are considered not ideal for long-term implantation because they contain high-cytotoxic elements like V, Ni or Co. Nickel is even considered an allergic carcinogen that shows one of the worst results in metal allergen tests [73]. Aluminum is known to be an element involved in neurological diseases, such as Alzheimer's disease and metabolic-bone disease [74]. While alloys with these elements are still one of the best materials in the field of prosthetics and implant dentistry, it is presumed that future development will be shifted towards β alloys with even more biocompatible elements like Nb, Ta, Mn or Mo [71].

One of the most basic biocompatible aspects of Ti alloys is their low modulus, as described in Fig. 15 (varying roughly from 50 GPa to 110 GPa), which is far lower than that of 316 L implant steel (around 210 GPa) and Co alloys (around 240 GPa), preventing bone resorption and implant loosening [52]. Since the interaction of the implant and human body occurs on the surface of the implant, surface treatment and roughness of the implant is considered to be critical when evaluating biocompatibility [75].

4.4 Surface treatment and osseointegration

One of the main deciding factors of a successful osseointegration of the implant is the quality of its surface. The geometry of the implant and its surface treatment play an important role during the bonding process in the early stages of osseointegration [76]. Directly after implantation, the bone in the peri-implant area starts to interact with the implant. Generally, there can be 2 responses after implantation. The first response means failure – the organism of the host creates a fibrous soft tissue capsule at the peri-implant area. This capsule does not provide a good mechanical fixation and eventually leads to clinical failure of the implant.

The second response means osseointegration – direct bone-implant contact without any disrupting interconnecting soft tissue layer.

There are several factors that decide whether osseointegration will be successful – for the sake of brevity, only the most important ones will be addressed. Generally, the most important parameters which are usually modified are surface roughness, geometry of the implant and chemical composition of the surface. The main indication for using an implant with modified surface is usually poor bone condition of the patient [76]. Reports have shown that titanium implants with roughened surfaces exhibit better bonding with newly formed bone tissue than implants with standard, machined surfaces [77], [78].

Surface rougness has been proven to play an important role in the bonding process [79], [80], [81]. The greater the surface area of the implant, the greater the interlocking between the implant surface and bone – bone ongrowth. However, there is a potential downside to having a very fine micro-roughness. As the surface area of the implant magnifies, so does the potential risk of ionic leakage [82]. Therefore, a moderate roughness of 1-10 μm is recommended for maximizing the interlocking between the new bone material and implant surface [78], [81].

Fig. 21: Manufactured functional titanium implant stems coated with porous titanium by means of plasma spraying. Conical stem with oblique beams (left), cylindrical stem with oblique beams (middle) and cylindrical stem with parallel beams (right). Images obtained from the 2015 TA03010886 project report submitted by CTU Prague, Faculty of Civil Engineering.

The most common methods of roughening the implant surface are titanium plasma-spraying (Fig. 21), blasting with ceramic particles, acid-etching and anodization. Some of the various surface geometry modifications are also presented in Fig. 22.

Titanium implants can also be coated with a bio-degradable layers of polymers, hydroxyapatite, collagen and many other specifically designed additional layers. These layers usually serve to improve the early healing process. They can also be used as antibiotics carriers, preventing early infections, which are usually connected with early failure in the implantation process. A well-designed bio-degradable polymer coating can improve the ongrowth of cells, prevent early infections and improve osseointegration. An example of different coatings applied on in-vivo test specimens is shown in Fig. 22.
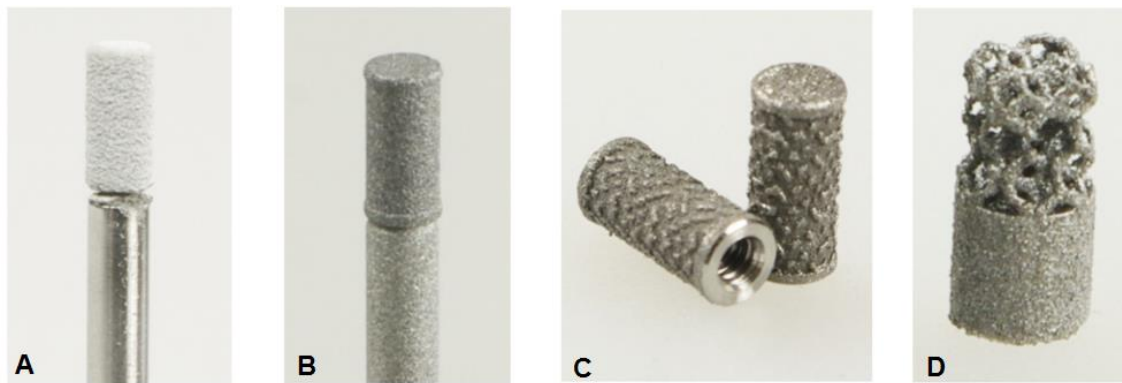
Fig. 22: In-vivo test specimen: A) Ti-6Al-4V with HAP (hydroxyapatite) coating, B) experimental Ti-35Nb-6Ta with PLA (polylactide), C) experimental 3D-printed specimen with COC (cycloolefin), D) experimental 3D-printed trabecular structure. Images obtained from the 2015 TA03010886 project report submitted by CTU Prague, Faculty of Civil Engineering.

5 Trabecular structure

5.1. Introducing the trabecular structure

The main reason behind creating complex structures, such as the trabecular structure, is simple – conventional morphology does not deliver well enough in terms of osseointegration and mechanical properties. Conventional implants have well-proven long-term success rates, but are still prone to failure in the early stages of the bonding process, as geometry and surface properties play an important role in osseointegration [76].

Trabecular structures are not yet commercially used in implant dentistry and there is very little data regarding their mechanical properties, characteristics of failure, fraction criteria, longevity or success rates, when compared to conventional homogeneous implants. It is a novel, perspective structure that cannot be machined, but rather 3D-printed and requires close attention and monitoring of its behavior. The advancement in the technology of 3D printing of metals makes it possible to create such complex geometric structures, which would not be achievable by conventional manufacturing methods. There are overall 2 main attributes in which the trabecular structure aims to exceed the quality of conventional homogeneous implants – osseointegration and low modulus.
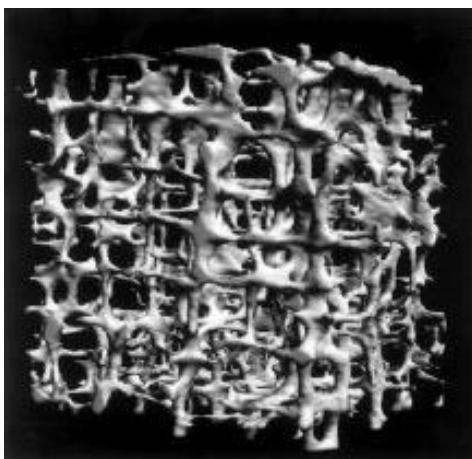
a) healthy trabecular bone architecture obtained by 3D micro-CT scan of cadaveric vertebral biopsy [83]
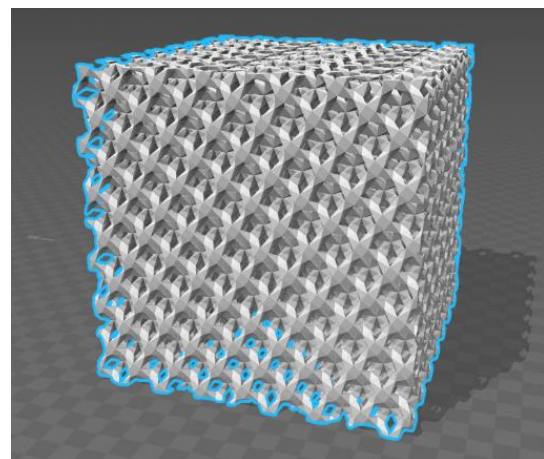
b) a 3D STL (stereolithography) model of trabecular structure used to create metal test specimen by means of 3D printing

Fig. 23: Healthy trabecular bone architecture (left) and its STL model (right).

a) whole implant body, consisting of both the trabecular and homogeneous structure
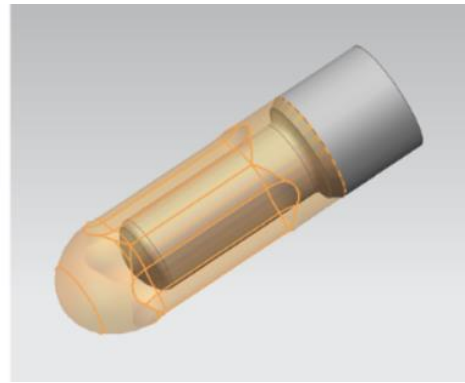
b) model of the whole implant, showing the homogeneous stem enveloped by an outside layer

Fig. 24: Images showing the final implant incorporating both the homogeneous (stem) and trabecular (casing) structures – left. Right – model of the structure. This is the implant that will be analyzed in the future with the help of the numerical model developed in this thesis. Please refer to chapter 7.7 Future prospects for further explanation.

5.2 Osseointegration and low modulus

The first attribute that can be improved by introducing the trabecular structure is osseointegration. The morphology of the trabecular structure resembles that of the trabecular bone (Fig. 23). The geometry of the trabecular structure forms the bearing scaffold for the ingrowth of bone cells into the implant [84], [85]. This interconnection is beneficial for long term stability at the implantation site [86]. With conventional implants, bone cells are only able to grow onto the surface of the implant. With the trabecular structure, however, the cells can grow inside and create an interconnected material comprising of both bone and metal bonded together. Therefore, the trabecular structure has a potential of much better bonding and creating a fluent material transition region. However, due to a lack of experimental data, this assumption is still to be proven true or false.

The second attribute is Young's modulus. While the reduced modulus of the material itself remains unchanged, the global modulus of the whole structure is expected to be dramatically reduced since the cross-section of the whole body is also reduced (Fig. 25). This reduction helps to smoothen the material transition region, where unwanted stresses often cause large deformations, leading to implant loosening. As shown in Fig. 24, the trabecular surface provides an interconnecting layer between the bone and the stem of the implant.
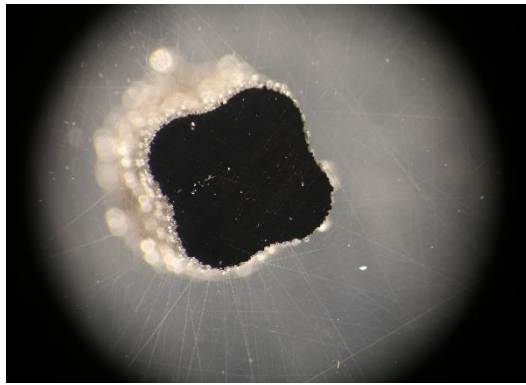
a) homogeneous (full) cross-section of an
   implant test specimen

b) trabecular cross-section of an implant
   test specimen

Fig. 25: Micrographs of full and trabecular cross-sections of an implant test specimen.
Note the difference between the cross-section area.

5.3 Stress shielding

Conventional implants of all kinds have one common shortcoming – stress shielding. Stress shielding is an unwanted factor that represents uneven distribution of stress between the implant, peri-implant area and bone. Naturally, the bone is provided by an evenly redistributed stress that provides all of its areas with sufficient loading to maintain its mass. By replacing bone with an implant, which has much higher value of modulus, we modify the stress distribution that occurs under load. Since the modulus of the bone is much lower than that of the implant (approximately 20-30 GPa [87] for bone and 90-110 GPa for conventional titanium implants [51]), stress is transferred into the implant, leaving the bone without sufficient stimulus.

At this point, the aforementioned Wolff's law plays an important role – the bone around the implant starts to remodel itself and deteriorate [38]. When the bone becomes overly porous, it is no longer able to hold the implant in position, making it eventually slip out, resulting in failure of the implant [88]. Note the difference between the strain energy density before and after implantation shown in Fig. 26 demonstrated on a human femur.

Stress shielding is an unwanted factor that is induced by multiple aspects. As previously mentioned, it is mainly caused by different material properties (modulus) of the bone and implant. Other factors that come into consideration are administration of anabolic agents, implant design and the biological compatibility of the implant material [89].
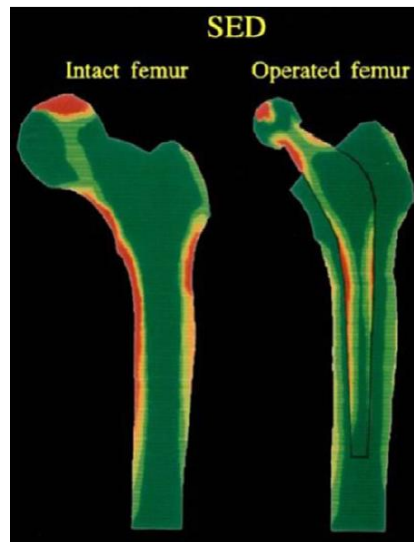
Fig. 26: Illustrated effects of stress shielding. Strain energy density (SED) of the intact femur (left) and the SED of the femur after implantation (right) show a different distribution. The levels of SED are greatly reduced at the proximal medial aspect of the femur after implantation [89]. This effect illustrated on an operated femur is similar to the effects of implants in jaws.

5.4 3D Printing technology

Conventional machining does not allow to create more advanced and complex geometric structures. The trabecular structure comprises of beams of equal length embedded into a 3D matrix, making 3D printing potentially the only technology available to produce it. The first step in creating a 3D-printed product is creating a 3D-model. This part is usually done using a computer-aided design (CAD) environment. Upon its completion, an STL model file (Fig. 23 b) is divided into thin cross sections [84], [85] and sent to the 3D printer to be processed. Up to this point, the process is similar to the common layer-by-layer 3D-printing of plastic.

What differentiates the process of printing metals from the standard technology is using a laser beam to melt down a layer of metal powder. During each cycle, the coater applies a thin layer of powder, which is processed by a laser at a pre-set melting point in a pre-determined order [90]. This process solidifies the loose powder into a 3D-layered object.

3D printing is a very modern and perspective method in manufacturing the bodies of implants. It allows for very complex structures, which would not have been conceivable with traditional metalworking. It also proves to be beneficial in terms of manufacturing speed and

storage, because there is no need to produce large batches of specific implants at once due to the long process associated with the calibration of the assembly line.
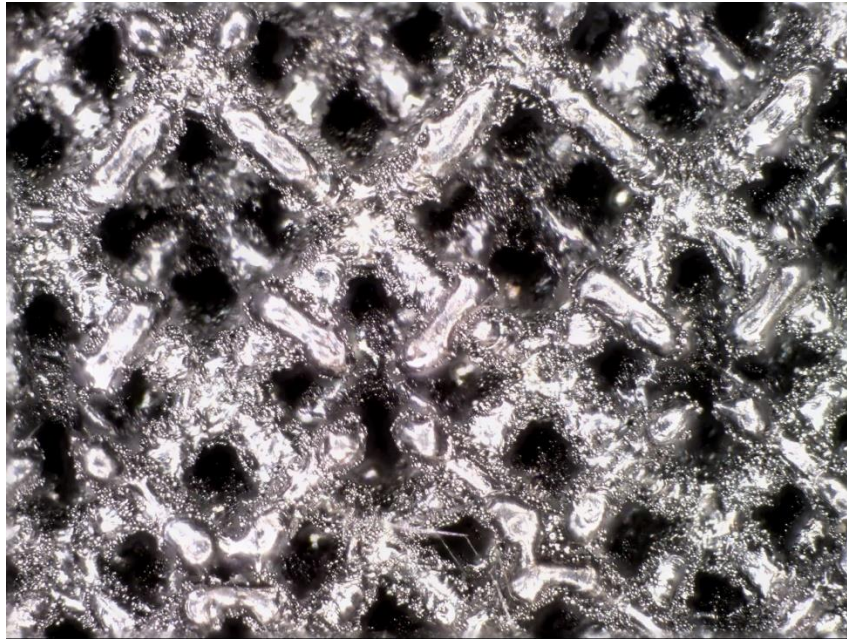
Fig. 27: Micrograph of a 3D-printed trabecular structure. Note the individual levels of beams embedded in the 3D trabecular matrix.

Despite the fact that the trabecular structure has many benefits, it also has its flaws. While observing the quality of the 3D-printed specimen, many geometrical imperfections associated with the printing technology were discovered. These imperfections are very hard to incorporate in any model as their occurrence seems to be purely random. The imperfections are shown in Fig. 28 and Fig. 29. They are, rather than a bad attribute of the structure itself, caused by the production process of 3D printing. They probably arise during the phase in which the machine applies a layer of powder and subsequently melts it by the laser beam. I expect these geometrical imperfections to be caused either by improper tracing of the laser beam, faulty metal powder dosage, or a combination of both. While the trabecular structure brings many benefits to the field of implantology, the technology of 3D printing still has to improve in order to provide stable, homogeneous outcomes and dependable products.

Since the imperfections did not seem to follow any particular pattern and were present (in different places) in all specimens, I decided not to incorporate them into the model as it is unsure what the outcome would be, had they been printed on a different machine. Also, this trend is not connected with the trabecular structure, but it is rather a production issue.
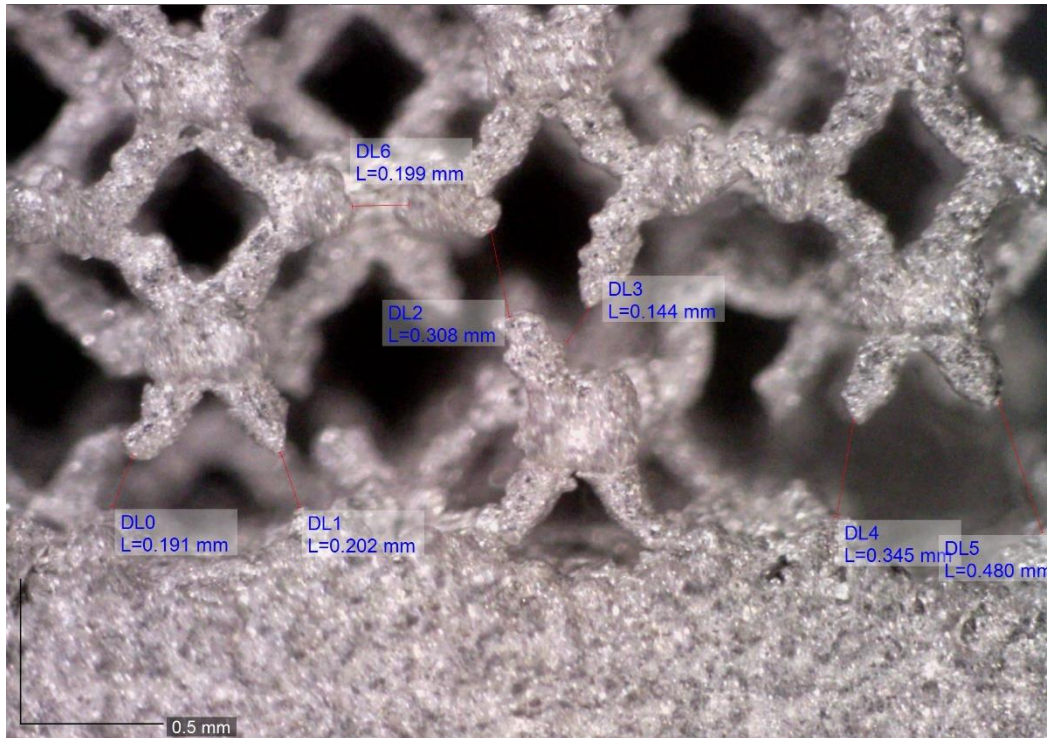
Fig. 28: Production imperfections at the interface of the homogeneous and trabecular cross-sections of the tensile test specimen. Note the faulty intersections of the beams as well as the disconnection of particular beams. Image provided with measured length of the disconnected areas.
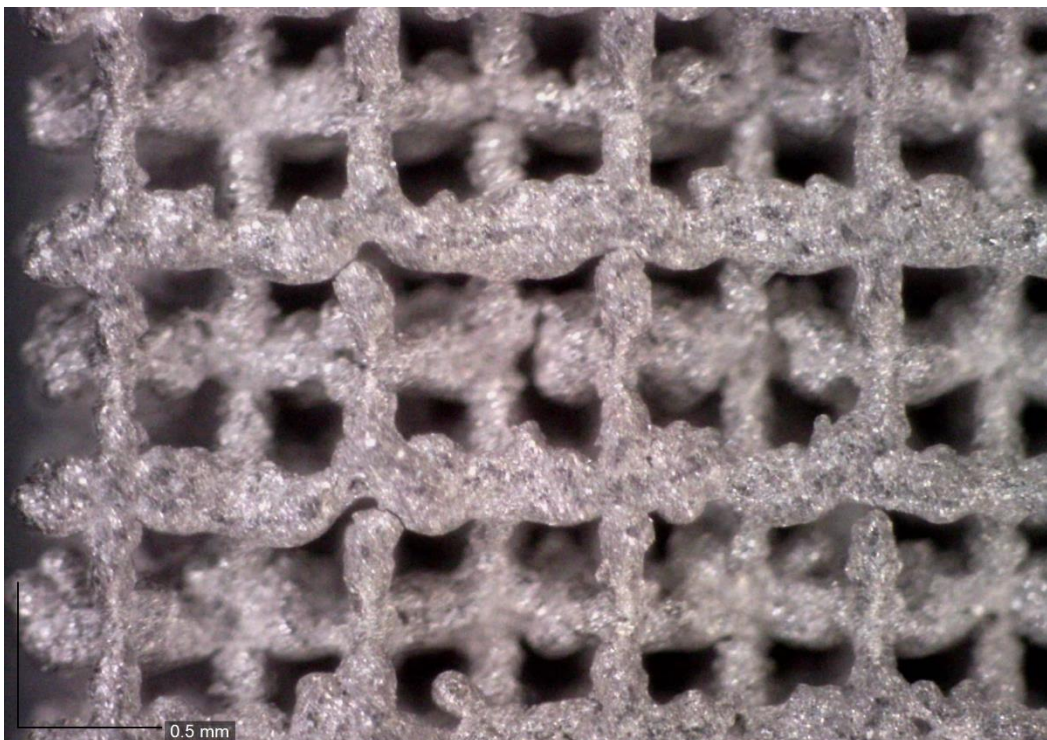
Fig. 29: Production imperfections inside the matrix of the trabecular structure. Note the imperfections of the intersections of the beams and different widths of individual beams.

5.5 Trabecular specimens for mechanical tests

A total of 12 specimens were created for the purpose of global mechanical tests – 3 for tensile and 9 for compression tests (as the compression failure characteristics are unclear and are expected to be much more heterogeneous). Two other specimens were created to investigate the micromechanical properties by means of naoindentation. The trabecular specimens were 3D printed using the M2 Cusing machine from the Concept Laser Company. The manufacturing of the specimens has been done in cooperation with ProSpon spol. s. r. o. A specialized input medium Rematitan CL was used for the printing of the test specimens. It is a Ti-6Al-4V titanium alloy powder provided by medical technology manufacturer Dentaurum. The 3D-printed compression and tensile test specimens are shown in Fig. 30.

a) compression test specimen   b) tensile test specimens
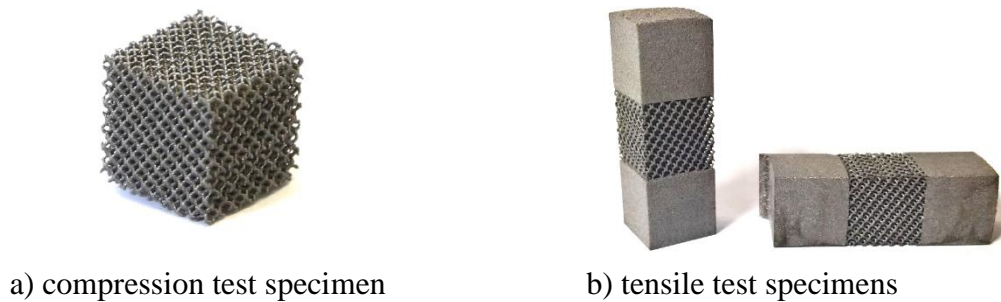
Fig. 30: Trabecular structure specimens for global mechanical tests.

For the purpose of mechanical tests, we used the 3D Dode-Thick [MSG] structures with dimensions of 14x14x14 mm (a cube for the compression test, Fig. 30 a) and a 14x14x42 mm (a block for the tensile test, Fig. 30 b). The tensile test specimen had a 14 mm trabecular middle section and end portions of homogeneous volume for ensuring a better anchor in the MTS Alliance RT-30 machine. The chemical composition of the material is shown in Tab. 4. It is a powder based on the well-known Ti-6Al-4V titanium alloy. This alloy has been chosen because it is already approved for use as a biomaterial and has a long history of great success rates in implants. Its material list is shown in Tab. 5.

Tab. 4 : Chemical composition of the Rematitan CL metal powder.

Component	Mass (%)
Ti	90
Al	6
V	4
Other elements <1 %: N, C, H, Fe, O	

Tab. 5: Material list of the Rematitan CL titanium powder used to create the test specimens. Courtesy of Dentaurum.

Yield Strength $R_{p0.2}$	950 MPa
Tensile Strength R_m	1005 MPa
Elongation at fracture A_5	10%
Modulus of elasticity E	115.000 MPa
Melting range Δ	1604-1655 °C
Density ρ	4.5 g/cm^3
Coefficient of thermal expansion TEC (25-500°C)	10.16e-6 K^{-1}
Colour	white
Metal-ceramic bond strength acc. to EN ISO 9693, 3-Pt.-bending test (min. 25 MPa acc. to EN ISO 9636)	37 MPa (Triceram, Dentaurum)
Type	4
Bicompatibility, L 929-Proliferation acc. to EN ISO 10993-5, -12	No deliberation of cell toxic active substances
Corrosion resistance, static immersion test acc. to EN ISO 10271 (max. 200 μg/cm^2 x 7d acc. to EN ISO 22674)	Ion release 1.41 μg/cm2 x 7d

6 Mechanical and in-vivo tests

To investigate the mechanical properties of the structure, we performed nanoindentation and tensile and compression (global) mechanical tests. While global mechanical tests do not require further preparation of the samples, the nanoindentation method demands a careful preparation of the transversal section and surface roughness elimination.

6.1 Nanoindentation

In order to prepare the trabecular samples for nanoindentation, they were submerged in epoxy resin and subsequently cut in the transversal plane in the MTH Mikron 3000 machine. This process was followed by progressive polishing using sandpapers of various roughness in the Struers LaboPol-5 machine. By incorporating this process, it is possible to achieve surface roughness levels of approximately hundredths of μm, which is enough considering the deformations caused by the indentor tip (approximately 400 nm). After this process, the samples were polished again using a polishing canvas and diamond paste Struers DP-Spray P. Finally, the samples were submerged into an alcohol-filled container and cleaned by ultrasound cleaner PS03000A. The section of the final polished ultrasound-cleaned sample is shown in Fig. 31.
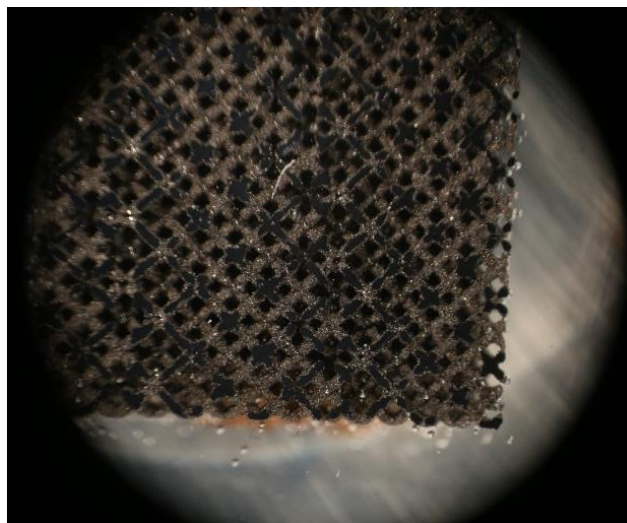
Fig. 31: Micrograph of a polished transversal section of the trabecular nanoindentation test specimen submerged in epoxy resin.

The nanoindentation tests were made considering reduced modulus of elasticity, hardness and contact depth and using the Oliver & Pharr method. The micromechanical analysis was performed using the CSM Instruments nanoindenter equipped with a Berkovich indenter tip. An image of the polished cross-section of the implant and a typical indentation matrix are shown in Fig. 32.

a) a polished cross-section of the trabecular specimen

b) a typical 3x3 indentation matrix with visible plastic deformation in the beams of the alloy
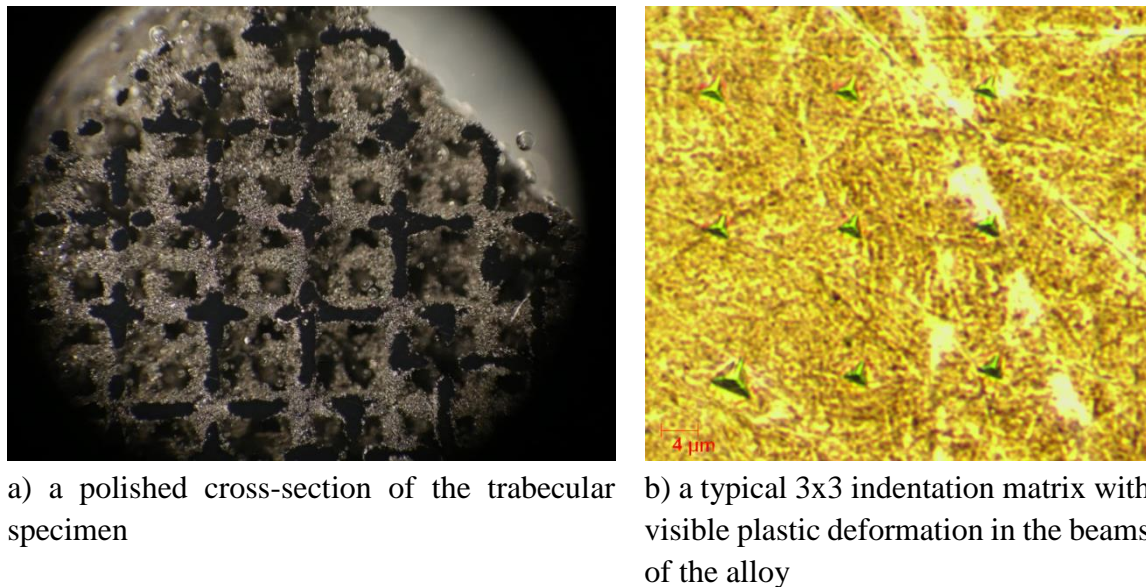
Fig. 32: An image of the cross-section of a trabecular specimen used for nanoinentation and an AFM image with visible indents in the beams of the trabecular structure.

The load program was set with consideration of eliminating surface tension and shear stiffness in the atomic material structure. The load program was set in the mode of directed force and repeated loading. For the purpose of this experiment, the maximum force applied by the indenter tip was set to a value of 20 mN. The whole load program consists of three phases – loading, constant force interval and unloading (Fig. 33). During the loading phase, the force gradually reaches 20 mN (10 seconds), then is constant throughout the constant force interval (10 seconds) and then goes down to a value of 0 mN during the unloading phase (10 seconds). One indent then takes 30 seconds to perform, then the device moves to another pre-set point in the indentation matrix (Fig. 32 b), recalibrates and approaches another loading phase. The whole cycle took approximately 3 minutes to perform. The shape of the matrices can be set arbitrarily; for this experiment, we chose the square matrix shape to maximize the indentable area inside the intersection of the beams.
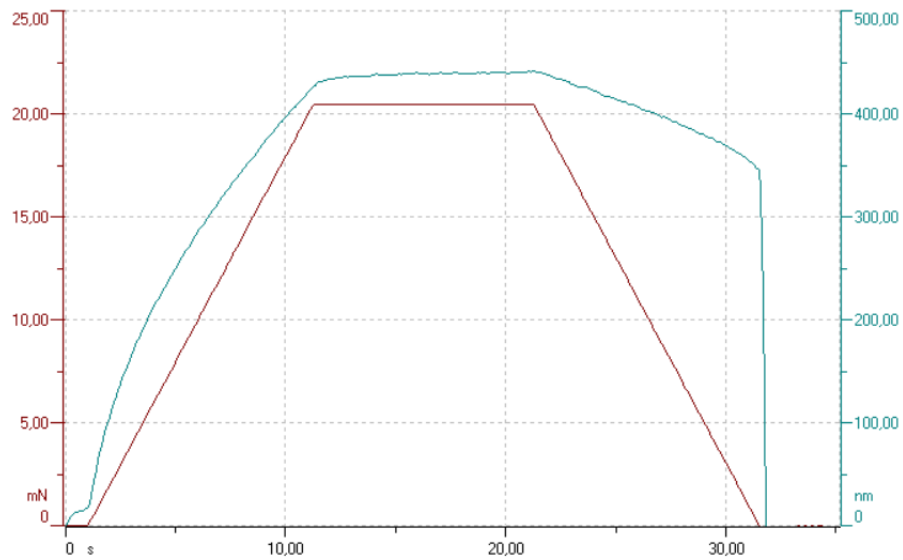
Fig. 33: The indentation load program obtained from one indent. Loading force (red) on the left vertical axis and displacement (teal) on the right vertical axis. Horizontal axis represents time.
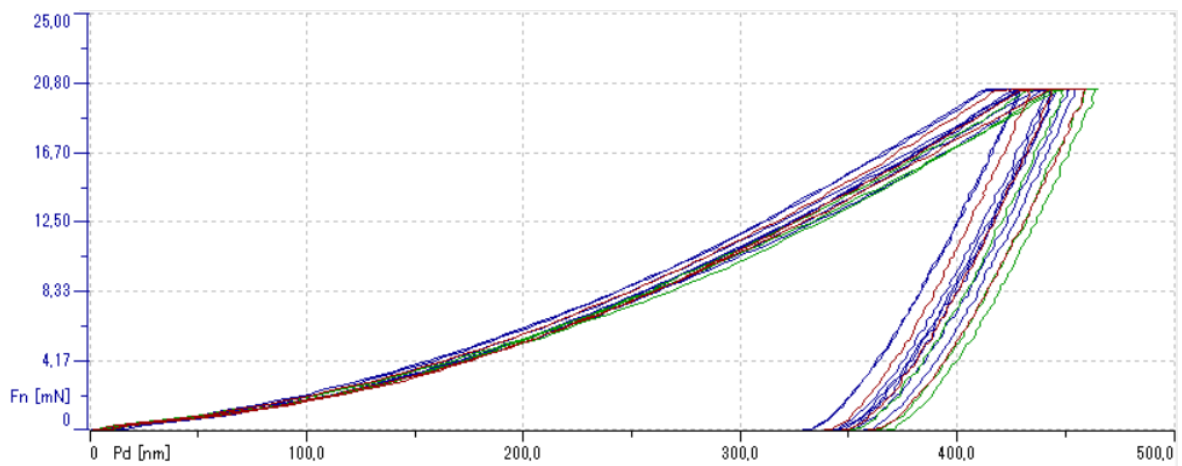
Fig. 34: Three sets of indentation curves obtained from indentation of the first specimen.
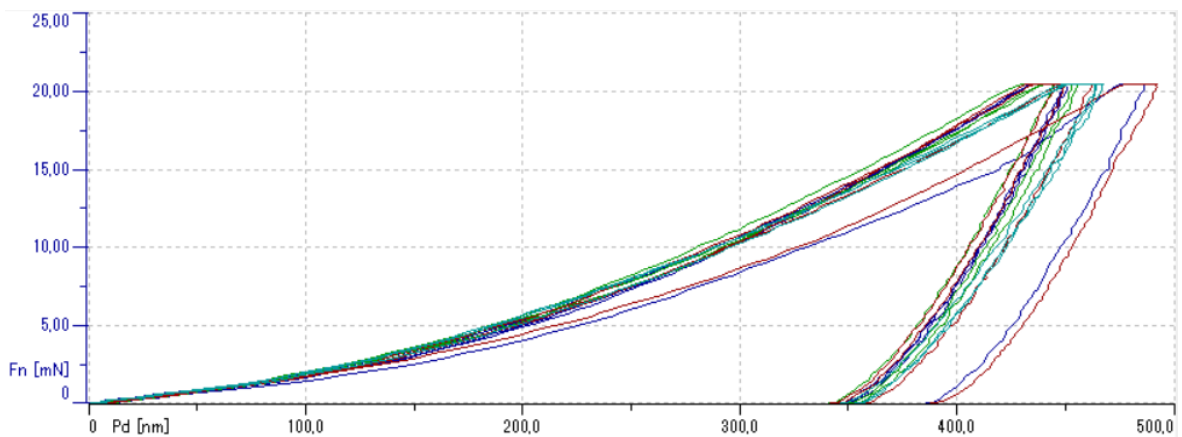
Fig. 35: Four sets of indentation curves obtained from indentation of the second specimen.

The two nanoindentation specimen were tested by a total of 7 indent matrices – three were situated in the first specimen and two in the second specimen (Fig. 34 and Fig. 35). The resulting mechanical properties can be seen in Tab. 6.

The three matrices in the first specimen contain a total of 17 indents. Three indents were taken out of the analysis (the first one in each set) as they did not have similar representative characteristics as the rest of the data. Similarly with specimen number two – it contained a total of 16 indents and two of them were not considered. This is a phenomenon I have encountered before while conducting nanoindentation tests of human dentin on the same indenter machine as a part of my Bachelor's thesis [87]. As the diamond tip moves across the cross-section of the sample, the first indent of a matrix it makes sometimes yields non-representative results. I attribute this shortcoming to the machine's need to recalibrate itself before performing a new matrix of indents in a different place, where roughness and distance from the default indenter position might be different.

It is very important to distinguish between results obtained by nanoindentation and global mechanical tests, especially when considering the trabecular structure. Nanoindentation represents the mechanical properties of the material on the micro level and global mechanical tests describe the properties of the whole tested specimen. While these two properties might be somewhat similar when testing a homogeneous specimen, it is vital not to mix them up when considering trabecular structure, where the values can vary as much as 100 times (Tab. 6 and Tab. 7).

Tab. 6: Mean values of reduced modulus E_r, hardness H_{it} and contact depth H_c in individual load cycles.

Physical property	Load cycle						
	1	2	3	4	5	6	7
H_{it} [MPa]	5191	5201	5188	5166	5191	5202	5191
Std. Dev.	251	200	281	343	379	404	395
E_r [GPa]	131	122	119	118	117	117	118
Std. Dev.	10	6	4	3	3	3	4
H_c [nm]	267	381	471	544	608	660	732
Std. Dev.	7	8	13	22	25	31	45

All results obtained by nanoindentation (Tab. 6) show that the values of reduced modulus E_r (the modulus of the material itself) fall in the range of 118-131 GPa. Considering the material list provided by the manufacturer (Tab. 5), where the value of E is 115 GPa, we can, with fair certainty, say that these values correspond. These material characteristics are also comparable to the conventional, machined Ti-6Al-4V implant material (Tab. 2).

6.2 Global mechanical tests

To investigate the global mechanical properties, we conducted compression and tensile tests. Global mechanical tests were performed using the MTS Alliance RT-30 machine. For the purpose of this experiment, we used the 3D Dode-Thick [MSG] structures with dimensions of 14x14x14 mm (a cube for the compression test) and a 14x14x42 mm (a block for the tensile test). The compression test specimen did not require any further modifications, but the tensile test specimens had a 14 mm trabecular middle section and end portions of homogeneous volume for ensuring a better anchor in the MTS Alliance RT-30 machine (Fig. 30 b). The specimens were tested beyond the point of failure.

The least squares method was used to determine the values of modulus E. Since the practice of making stress-strain diagrams is very common and well-known, I will not be addressing it in detail but rather move the explanation to chapter 7.2 Methodology. Diagrams showing the stress-strain relations of the specimens obtained by tensile and compression tests are shown in Fig. 36 and Fig. 37, respectively.
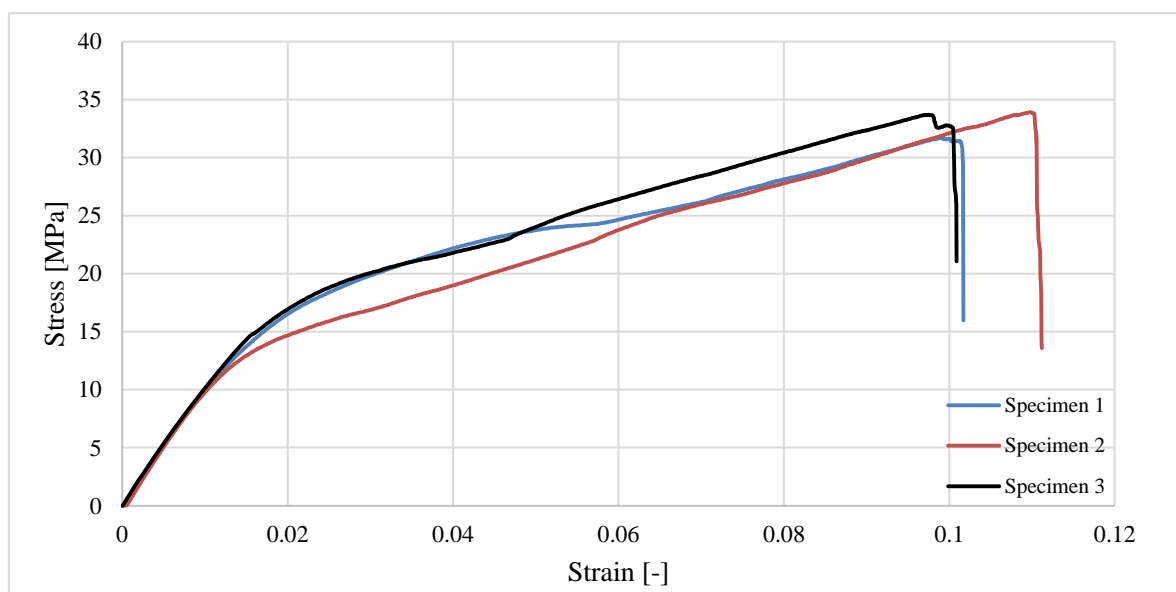
Fig. 36: Stress-strain relation diagram of the tensile test specimens.

From the linear part of the curves in the diagrams shown above and below, I was able to calculate Young's modulus of the whole trabecular specimen (Tab. 7) as the tangent of the stress-strain diagram. I have only considered the linear part of the curves because Young's modulus cannot be determined this way in the range of plasticity. For strain, these values range approximately from 0.00 to 0.15 for the tensile test and from -0.025 to -0.05 for the compression test. These values represent properties of the whole specimen, contrary to the nanoindentation experiment, where obtained values represent only the material characteristics at the micro level.
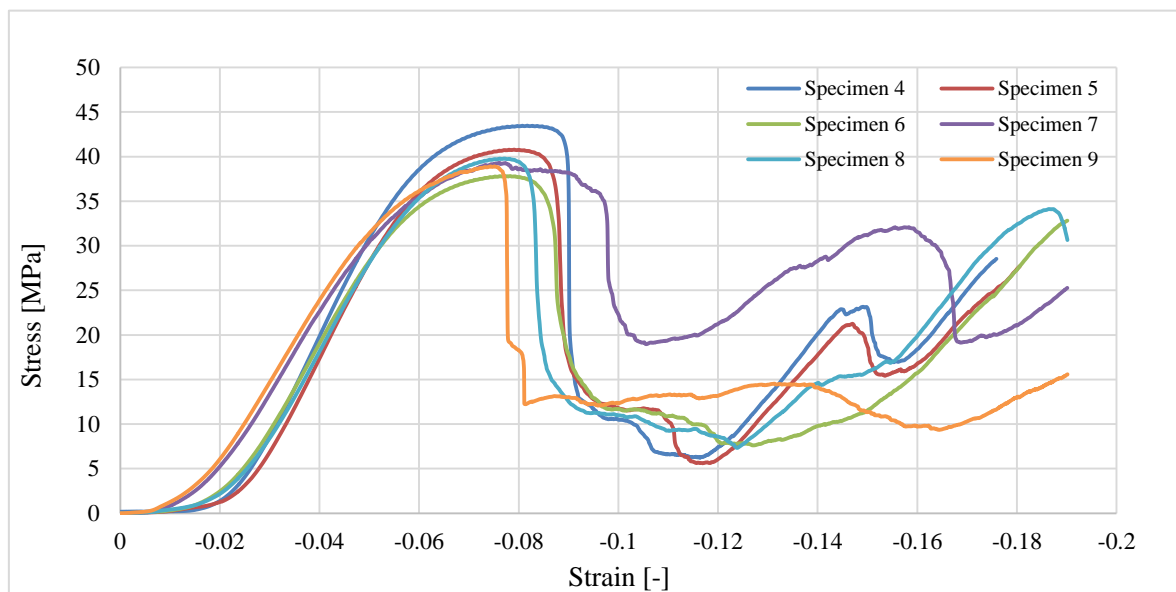
Fig. 37: Stress-strain relation diagram of the compression test specimens. Note the very heterogeneous nature of compressive deformation beyond the failure of the specimen. This fact can be attributed to the individual layers of the trabecular structure locking into one another in a random fashion.

Tab. 7: Values of Young's modulus obtained by global mechanical analysis.

	Young's modulus E [MPa]									
Specimen	1	2	3	4	5	6	7	8	9	Mean
Tens. test	964.7	975.9	982.2	-	-	-	-	-	-	**974.3**
Comp. test	-	-	-	1114.2	1080.6	947.2	818.8	999.6	803.8	**960.7**

As shown in Tab. 6 and Tab. 7, the values of modulus vary dramatically. By introducing the trabecular structure, the modulus of the structure was lowered more than 100 times. This outcome is purely experimental as the structure does not have any documented material tests and no experiments performed whatsoever. However, I believe that the values of modulus do not necessarily need to exactly match human bone as more aspects come into consideration.

If the structure had its beam structure and width experimentally manipulated in order to match the modulus of human bone, it would not necessarily be prolific as more data and in-vivo experiments are still needed. Porosity, beam width and surface morphology are vital parameters in order to fully osseointegrate the implant and induce bone ingrowth, which is one of the main potentials of this structure. Therefore, observing the results from in-vivo tests can be a far more productive approach than exactly matching the properties of the structure and human bone.

6.3. In-vivo tests

As an addition, I have decided to include a chapter in my thesis very briefly reviewing the results obtained from in-vivo tests of the trabecular specimens. Because this topic is beyond the limits of this thesis and my knowledgeability, consider the following information and figures simply as an additional graphic illustration of the aforementioned text.

I have attended in-vivo tests of the trabecular implant specimens. The tests took place at the Institute of Animal Physiology and Genetics AS CR, v. v. i. in Liběchov, Czech Republic and were carried out on laboratory pigs. The whole purpose of the in-vivo tests was to observe the healing process and ultimately determine the osseointegration of the trabecular implant specimens after 6 months following implantation. The implants were placed in the proximal area of the femur of pigs. There was a total of 34 implants placed in 4 pigs. Six months after the operation, the bones were extracted and tissue bars 3 cm long and 1-3 cm wide were made in order to examine the individual bonding abilities of various implant shapes. Subsequently, the samples were cut in half and their surface was prepared in a similar fashion as the aforementioned nanoindentation specimens.

There were 4 types of implants tested, but for the sake of brevity, I will only be addressing the trabecular implant specimens.
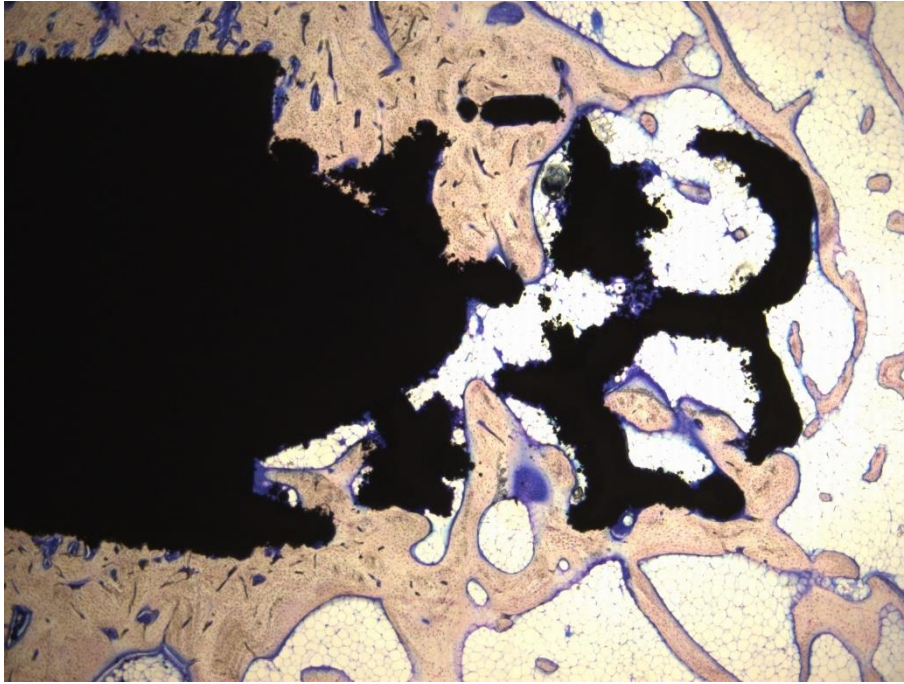
a) trabecular specimen n.1
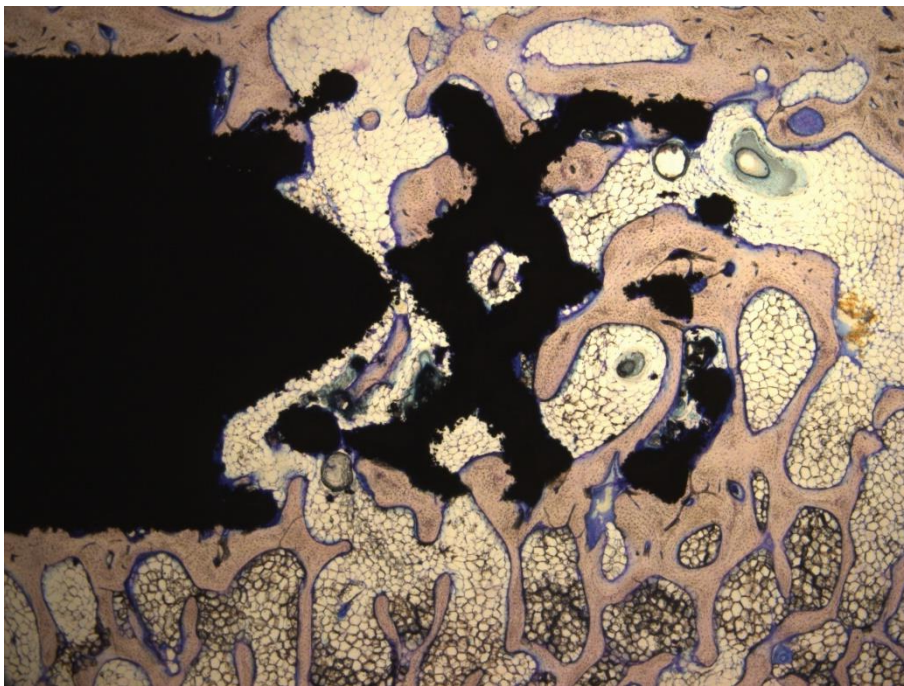
b) trabecular specimen n.2

Fig. 38: Two micrographs of longitudinal sections of extracted trabecular specimens. The samples were colored using Giems solution azur-eosin-methylene blue. White and light yellow color represents beams of newly formed bone, orange represents fibrous tissue and black color represents the trabecular implant [91].

To quickly evaluate the outcome of these in-vivo tests, it was discovered that the bone-implant contact of the trabecular structure was inferior to that of the conventional

homogeneous implants. However, it was still better than the remaining 2 groups of experimental implants [91]. Bone-implant contact is a major indicator of osseointegration, but more tests will be needed in order to gain more data and evaluate the experiments in different conditions and with different parameters.
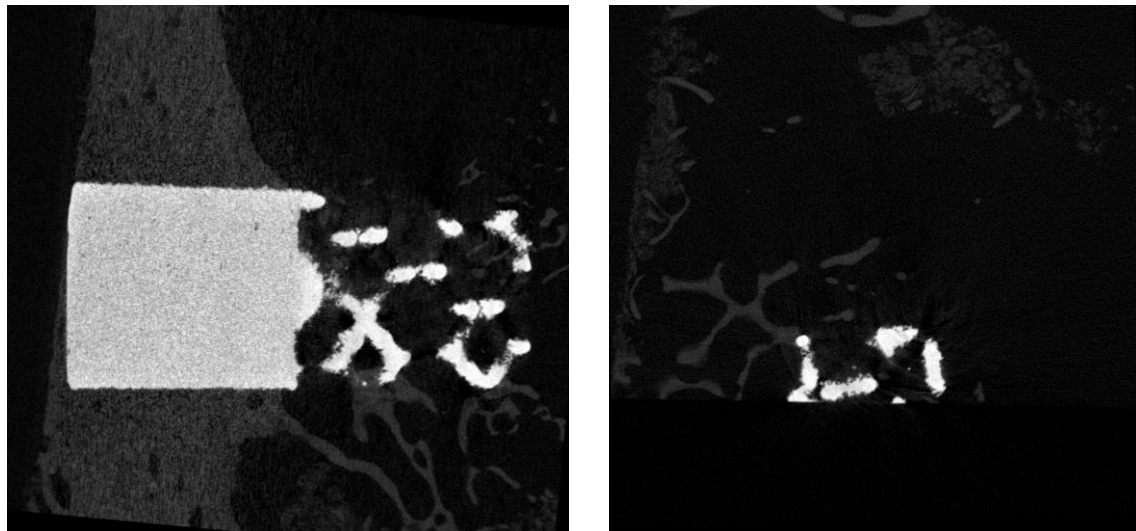
a) longitudinal section of the specimen   b) transversal section of the specimen

Fig. 39: Micro-CT scans of the trabecular implant inside a tissue bar it was extracted with. Visible bone and fibrous tissue in the background. White areas represent the body of the implant.
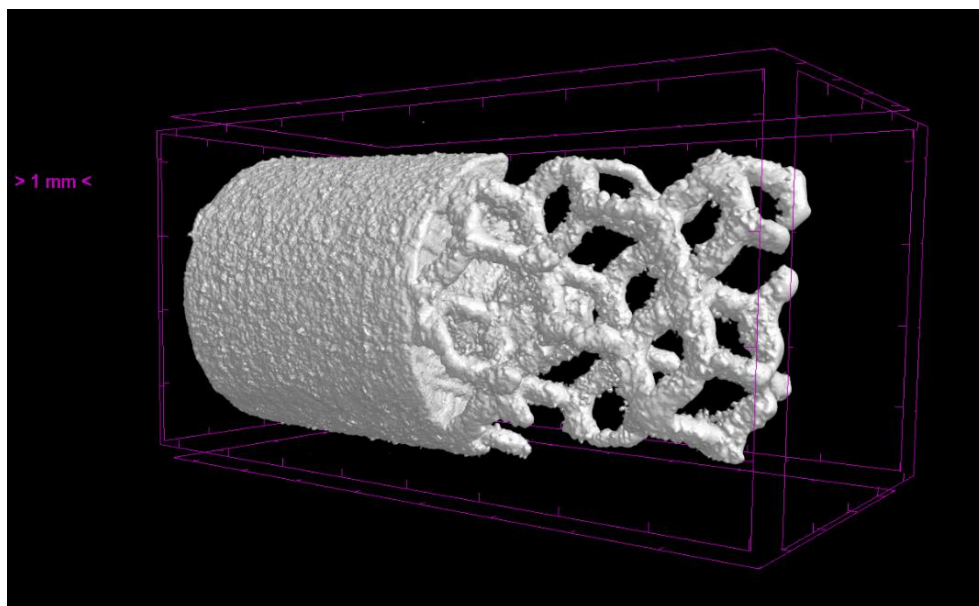
Fig. 40: Scaled micro-CT scan of the implant specimen with a trabecular end portion.

7 Numerical model

7.1 Purpose of the model and its introduction

The idea behind the development of a numerical model of the trabecular structure is to create a virtual material that will be utilized in various numerical tasks. Because there is no evidence of any numerical model of this structure, it is also a very challenging issue with no expectable results. Such model can then be utilized to determine the stress distribution in the bodies of whole implants consisting of both the trabecular and homogeneous cross-sections. The numerical approach was non-linear.

The future purpose of the model is twofold – the first one is to apply the material characteristics to the trabecular structure and fully represent its behavior. The second is to apply these characteristics to a homogeneous structure that will then represent the trabecular structure as a homogeneous material with the mechanical properties of the trabecular structure. The first approach is able to directly characterize the behavior of the structure and is my primary goal and concern. However, considering the complexity of the structure and the many problems that had arisen during the process of the numerical analysis, it is also possible that the whole process will be much more time-consuming. Because of that, I also consider the application of the trabecular properties onto a homogeneous structure a viable and functional alternative.

With the numerical model at hand, it will be possible to evaluate the stress distribution throughout implants of different shapes and structures. This comparison can then be used to manipulate the shape of the trabecular structure, structural portions of implants, width of the beams and their distance. Such comparison will lead to implant shapes that will have smoother stress distribution throughout their bodies, reduced stress-shielding and unwanted stress concentrations.

7.2 Methodology

My approach in the development of the model was to try to imitate the process of the tensile mechanical test to the best of my abilities. For this purpose, I used the Ansys Workbench 16.2. software for a finite element method analysis. Because I had at my disposal the test data from the MTS Alliance RT-30 test machine, I had full knowledge of the force-displacement relations. Knowing the exact dimensions of the specimens, I was able to recalculate the force into stress by using this simple formula:

$$\sigma = \frac{F}{A} \tag{1}$$

where σ represents stress, F represents the time-dependent load applied by the machine and A represents the cross-section area of the specimen. The dimensions of the tensile test specimen are 14x14x42 mm (Fig. 30), so the cross-section area equals 196 mm^2. The strain has been calculated using another simple formula:

$$\varepsilon = \frac{D}{L} \tag{2}$$

where ε represents strain, D represents the longitudinal displacement (extension) and L represents the total length of the trabecular middle portion (14 mm).

Considering the fact that the values of modulus of the homogeneous end portions (around 120 GPa) and the trabecular middle portion (around 1 GPa) vary approximately 100 times (Tab. 6 and Tab. 7), I have decided to attribute all deformation to the trabecular middle portion, since its low stiffness is likely to represent nearly all the deformation induced by the tensile test. This assumption can also be supported by the fact, that the end portions were anchored in the MTS Alliance RT-30 test machine, so most of their length represented rigid support.

Tab. 8 explains the manipulation with the experimental data. This data has also been used to produce the stress-strain diagrams shown in chapter 6.2 Global mechanical tests. The machine was recording the loading force and longitudinal displacement in 0.1 s long time steps. The whole experiment took about 430-470 seconds till failure of the specimen for all three specimens. The amount of data can then be, in my opinion, considered sufficient as

more than 4,000 individual force-displacement points were recorded for each specimen. This data was then used to calculate stress and strain and the displacement was also utilized in the numerical analysis in the loading program.

Tab. 8: Withdrawn part of the experimental data obtained from the tensile test. The first three columns were obtained from the loading machine and strain and stress were calculated. Total time range was 0-430 seconds.

Load [N]	Time [s]	Displacement D [mm]	Strain ε [-]	Stress σ [kPa]
57.96	5.3	0.00523	0.00037	295.70
63.76	5.4	0.00557	0.00040	325.32
67.80	5.5	0.00580	0.00041	345.91
72.94	5.6	0.00615	0.00044	372.16
78.79	5.7	0.00651	0.00047	401.99
84.87	5.8	0.00686	0.00049	433.03
90.93	5.9	0.00723	0.00052	463.91
96.69	6.0	0.00760	0.00054	493.30
103.12	6.1	0.00795	0.00057	526.10
109.09	6.2	0.00834	0.00060	556.59
115.18	6.3	0.00871	0.00062	587.63
121.44	6.4	0.00906	0.00065	619.58
127.36	6.5	0.00943	0.00067	649.81
132.65	6.6	0.00979	0.00070	676.79
139.34	6.7	0.01014	0.00072	710.93
144.82	6.8	0.01051	0.00075	738.89
151.01	6.9	0.01085	0.00078	770.44
156.25	7.0	0.01119	0.00080	797.17
161.69	7.1	0.01152	0.00082	824.93
166.88	7.2	0.01185	0.00085	851.40
172.20	7.3	0.01216	0.00087	878.55
177.40	7.4	0.01249	0.00089	905.12
182.27	7.5	0.01280	0.00091	929.96
187.36	7.6	0.01310	0.00094	955.91
192.35	7.7	0.01343	0.00096	981.36
197.78	7.8	0.01374	0.00098	1009.10

With this data at hand, I was able to use the least squares method to determine the values of modulus *E* of the trabecular specimens, which are listed in chapter 6.2 Global mechanical tests in Tab. 7. Applying the least squares method is a commonly known practice, so for the sake of brevity, I will leave its explanation out of this thesis.

The displacement provided by the loading machine was recorded (Tab. 8) for the absolute time frame (430-470 seconds for all specimens) and subsequently used as a

displacement load in the numerical loading program to simulate the exact process of the tensile test. This procedure will be shown and explained in chapter 7.6 Analysis settings and curve-fitting.

7.3 Geometrical model

In order to numerically simulate the loading process, it is mandatory to provide a geometrical model. I already had at my disposal the geometry used to 3D-print the trabecular specimen (Fig. 41 a). This STL model, however, was not suitable for numerical analysis because of its size. Had this model been meshed, loaded and analyzed, it would take several hours to compute, using a regular four-core PC processor. Such a lengthy analysis was not an option for this specific issue, since the analysis had to be performed numerous times in order to precisely curve-fit the tensile test. The analysis would not even be precise as the number of nodes in the mesh is limited in the Ansys academic license.

I decided that performing the analyses on a smaller model will be a better, more time-conserving approach. I swapped the model shown in Fig. 41 a) for a smaller model shown in Fig. 41 c). Since the only other model structure available was the basic structure of the single element (Fig. 41 b), I used it to create a model consisting of these basic elements. To scale it down in comparison to the default model, I used three of these elements per edge of the imaginary circumscribing cube of the structure, as opposed to seven elements per edge.
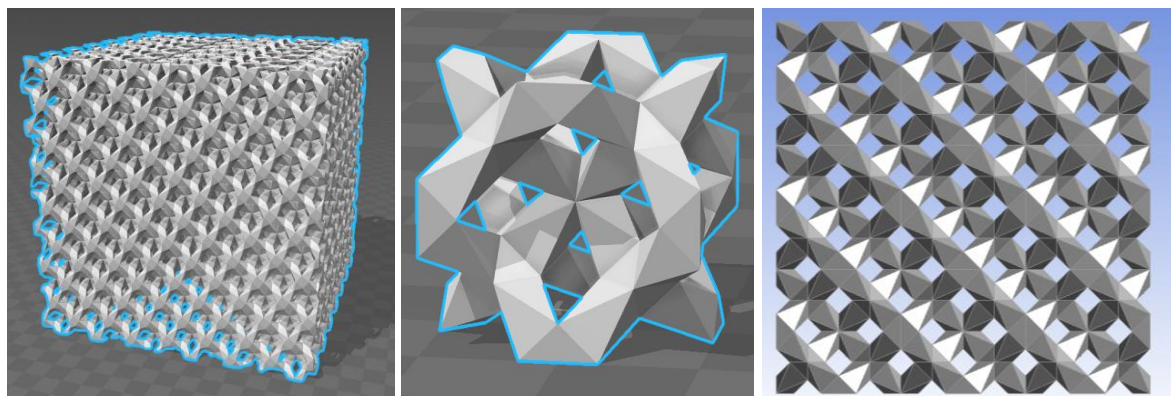
a) the former STL model used for 3D printing, consisting of seven basic elements per edge

b) the basic STL element

c) the new 3D model created in Design Modeler of Ansys Workbench, comprising of three basic elements per edge

Fig. 41: The 3D STL files used for 3D printing (a, b) and a smaller, newly created geometry utilized in the numerical analyses (c).

This step has proven to be very saving with regard to computation time. My former estimate was that it will need to be performed approximately 20 times, which was almost true as approximately 30 curve-fitting analyses needed to be performed to imitate the tensile test experiment. The environment I used to create the geometry was the Design Modeler of the Ansys Workbench software.

7.4 Meshing

With the geometry prepared, the next step in the numerical analysis was to create a proper mesh. While performing this task, I ran a couple of simple computations with elementary loads. The purpose of these computations was to determine how much does the size of the elements and their quantity influence the computation time. As a result of these mini-computations, I chose to incorporate a mesh that covers every single beam of the structure by a minimum of three elements. This quantity seems to be small enough in regard to computation time and also great enough to provide the necessary precision of solution. I also tried variants with more elements per the width of a beam, but have concluded that computation times were increasing so quickly that such an environment would have been absolutely unusable for the curve-fitting process. Also, I ran into limitations of the academic license, which restricts the maximum number of mesh nodes in a model.
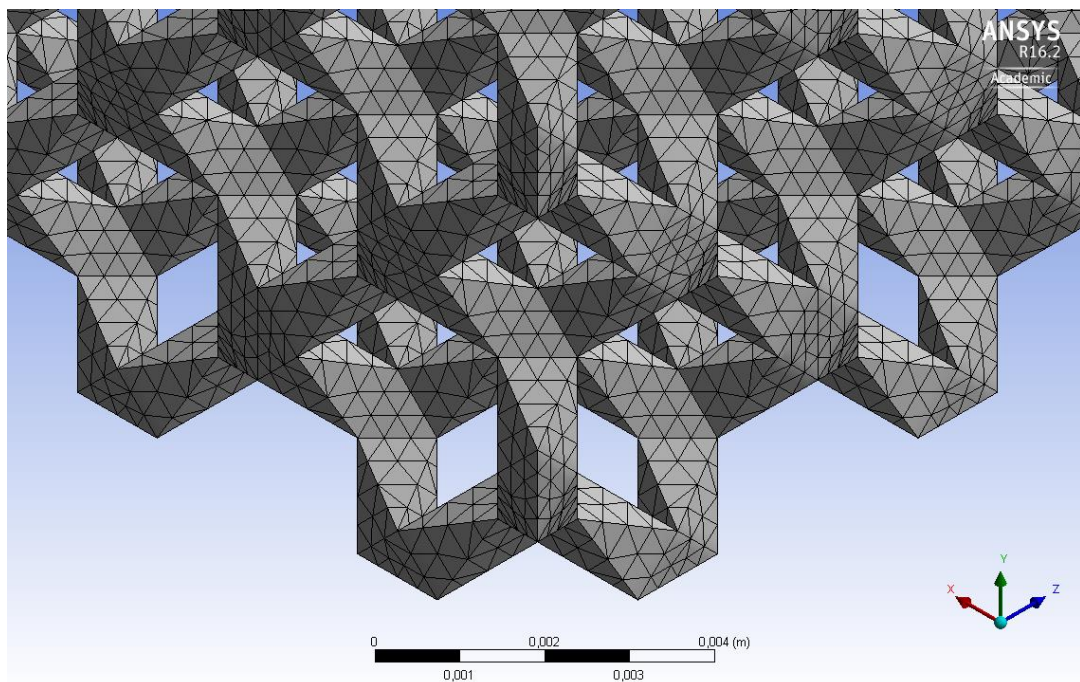
Fig. 42: The FEM mesh of the trabecular structure generated by the Ansys Workbench software. The mesh elements are tetrahedrons.

The elements used in the mesh were tetrahedrons. In order to achieve the desired number of elements per beam width, I specified the maximum surface area of individual elements to $4*10^{-4}$ m^2. To prevent the elements from spanning too large areas and have atypical shapes, I also specified the maximum inner angle of the triangles to 120°. There were a total of 78292 elements and 153827 nodes in the mesh (nearing the maximum numbers of the academic license).

7.5 Load program

With the geometry successfully meshed, setting a load program was the next step in the process. In order to withstand a load and induce a mechanical response, the geometry needs to be properly constrained. As the geometry is a rigid 3D body, it has 6 degrees of freedom. These degrees can all be constrained by fixed supports on one side of the trabecular structure that covers all faces which would be in contact with either the homogeneous structure or a machine anchor.
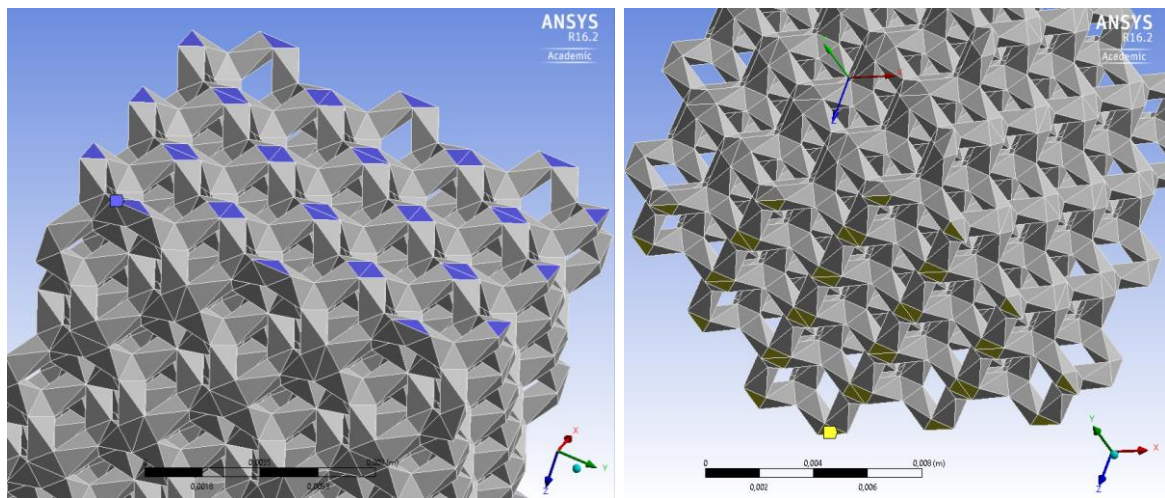
a) image showing the fixed support applied on blue faces of one side the structure

b) image showing the displacement load applied on the yellow faces of the structure on the opposing side in the direction facing out from the structure

Fig. 43: Images showing the geometry with applied supports and loads.

The provided load has been implemented in the form of tabular data as displacement of the specimen n.3 obtained from the tensile test. For this particular specimen, the test took

420 seconds until failure. I have decided to abbreviate this process and include only every tenth value of displacement, shortening the process into 42 steps. This reduction has been done because my computer has been having difficulties handling so many changes in load (effectively freezing for several minutes by merely accessing the data) and I also observed that computation times are rapidly increasing. Knowing that the displacement is almost a linear curve (Fig. 44), this reduction of load points did not interfere with the precision of the analysis.
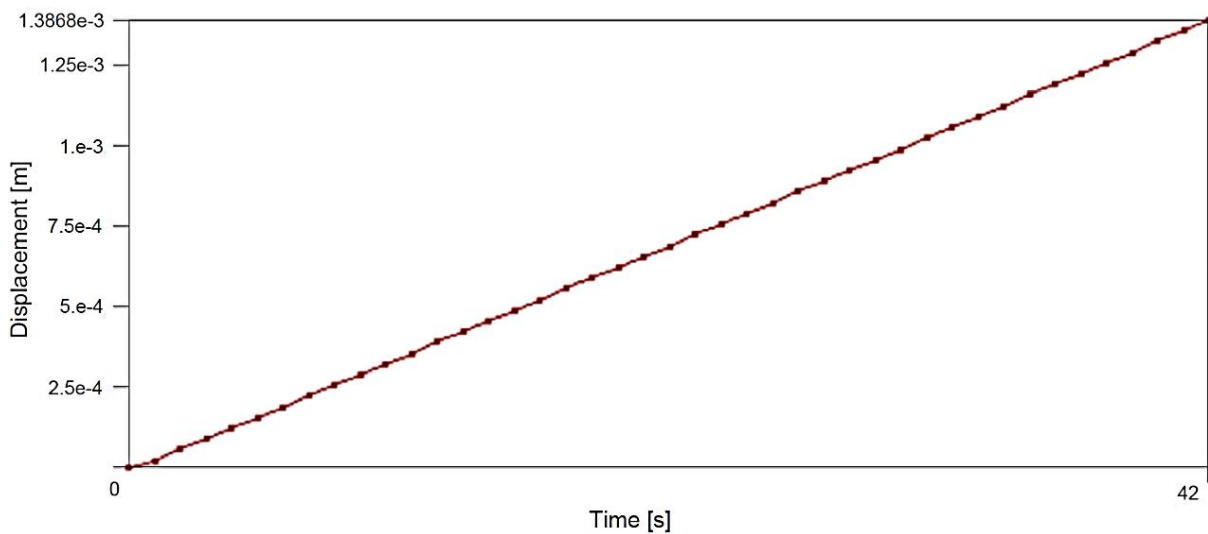
Fig. 44: The applied displacement load. The displacement was applied as a uniformly distributed load on all selected faces of the trabecular structure, as shown in Fig. 43 a). The total range of displacement load applied was 0-1.3868 mm. The corresponding maximum force for the top range displacement value was 6396.4 N.

Note that no further shown stress-strain diagrams show failure of specimens beyond the strain limits or ultimate strength, as specified in Fig. 49. Also, the stress values shown Fig. 45, Fig. 46 and Fig. 47 show stress values exceeding the ultimate stress. This is an acknowledged fact associated with the solution – the Ansys Workbench software cannot, by default, provide a solution that would deliver the failure of the model (at least not for a bilinear plastic model with isotropic hardening). Modeling the failure is a rather advanced technique attained by implementing the *ekill-ealive algorithms*. These algorithms assign a great reduction coefficient to every element in the stiffness matrix that has its strain or stress limits exceeded at the end of a computation step/substep (iteration). This significant reduction then nearly eliminates the element from the solution, thus simulating the failure of

the element. The fact that the failure of the model is not attained is fully acknowledged and will be addressed in detail in chapter 7.7 Future prospects.
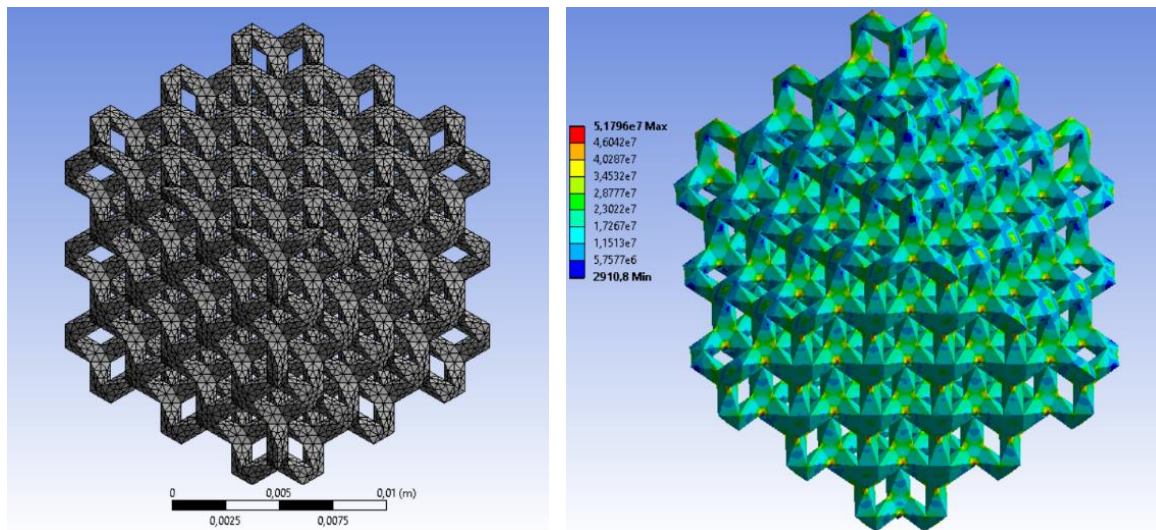
a) the fully meshed model before loading

b) the model as loaded with displacement load, isolines show equivalent (von-Mises) stress distribution in Pa

Fig. 45: Figures showing the model before and after applying the load. Note the stress distribution on the right as well as acknowledged stress values beyond the stress limits.

Images shown in Fig. 46 and Fig. 47 show a detailed von-Mises stress distribution throughout the structure. As expected, the greatest concentrations of stresses are located in the centers of intersections of beams and around sharp edges of the structure.
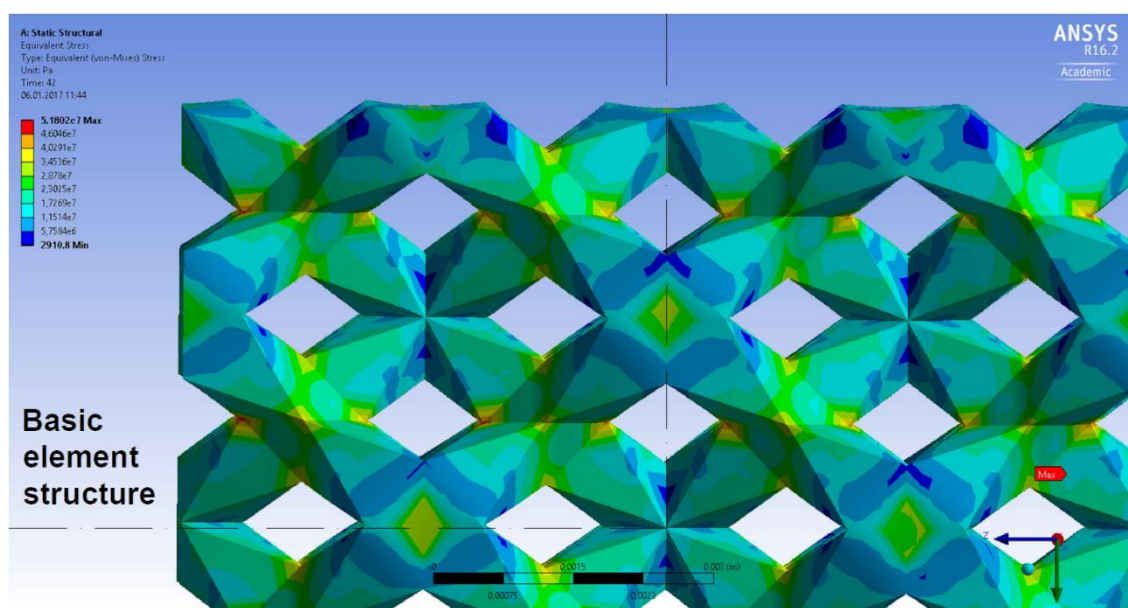
Fig. 46: A detailed von-Mises stress distribution of the model on the ZY plane. Dash-dotted line shows the single basic 3D element (Fig. 41 b).
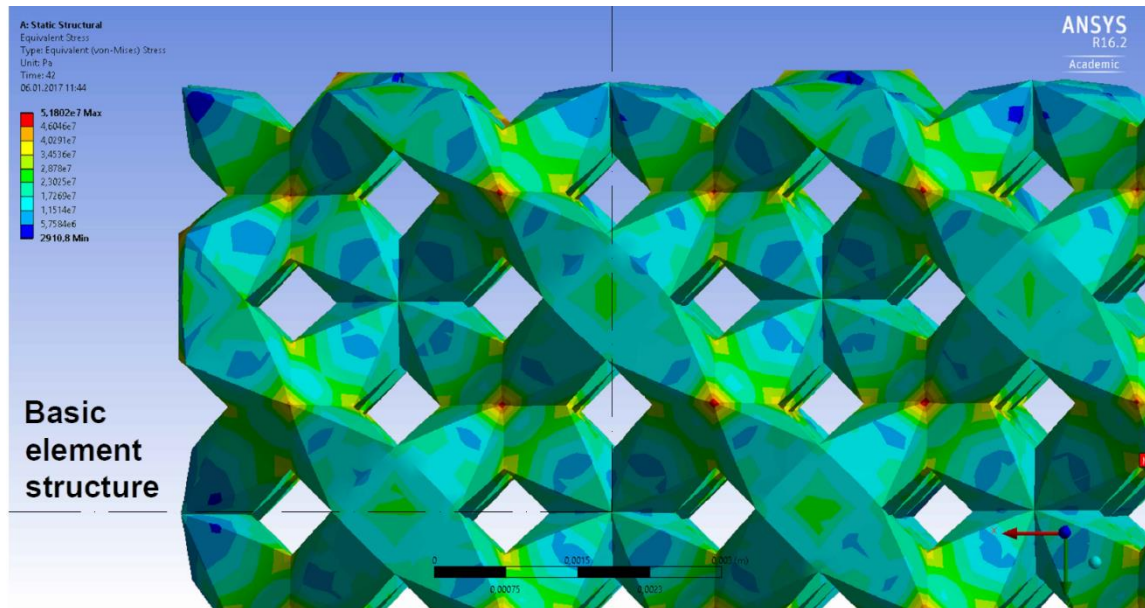
Fig. 47: A detailed von-Mises stress distribution of the model on the XY plane. Dash-dotted line shows the single basic 3D element (Fig. 41 b).

7.7 Manipulating material properties

In order to enter the curve-fitting process, one must first provide material characteristics and apply them onto the created geometry. Since the material I tested was made from a Ti-6Al-4V powder, I conveniently utilized the Ti-6Al-4V material provided by the Ansys Workbench material library introduced by Steinberg [92].

Unfortunately, the source of the equations of the material model is not available online to my institution, so they cannot be addressed in this thesis. The Ti-6Al-4V material model is, by default, implemented without any specified material characteristics aside from density, as shown in Fig. 48. It is then up to the user to define any required properties.

Fig. 48: The empty material characteristics list of the Ti-6Al-4V material model from the Ansys Workbench material library.

By experimentally manipulating the values of additional properties, I was able to affect the slope of the curve. The properties were gradually added and changed multiple times in

order to fit in the yield strength, ultimate strength and their corresponding strain values. The final values I specified at the time of the last computation are shown in Fig. 49.

	Properties of Outline Row 5: TI 6%AL4%V		
	A	**B**	**C**
1	Property	Value	Unit
2	Density	4419	kg m^-3
3	⊟ Isotropic Elasticity		
4	Derive from	Young's Modulus and Poisson's Ratio	
5	Young's Modulus	1,3E+09	Pa
6	Poisson's Ratio	0,342	
7	Bulk Modulus	1,3713E+09	Pa
8	Shear Modulus	4,8435E+08	Pa
9	⊟ Field Variables		
10	Temperature	No	
11	Shear Angle	No	
12	Degradation Factor	No	
13	⊟ Bilinear Isotropic Hardening		
14	Yield Strength	1,68E+07	Pa
15	Tangent Modulus	2,65E+08	Pa
16	Tensile Yield Strength	1,68E+07	Pa
17	Compressive Yield Strength	1,68E+07	Pa
18	Tensile Ultimate Strength	3,4E+07	Pa
19	Compressive Ultimate Strength	3,4E+07	Pa
20	⊟ Orthotropic Strain Limits		
21	Tensile X direction	0,1	
22	Tensile Y direction	0,1	
23	Tensile Z direction	0,1	
24	Compressive X direction	-0,1	
25	Compressive Y direction	-0,1	
26	Compressive Z direction	-0,1	
27	Shear XY	0,1	
28	Shear YZ	0,1	
29	Shear XZ	0,1	

Fig. 49: Full material specification given at the very last computation of the curve-fitting process. Note that some of these properties were changed approximately 30 times in order to achieve the desired curvature.

Since the process of manipulating the material characteristics, analysis settings and other variables intertwine together, I will leave the detailed description of the process to chapter 7.6 Analysis settings and curve-fitting, where I will refer to the aforementioned values and properties given in Fig. 49.

7.6 Analysis settings and curve-fitting

Since there is only a single load, the analysis is not complex and does not require additional time-separated intervals (unlike, for example a gasket assembly analysis with

tightening of bolts, subsequent thermal load etc.). It was performed in one computation step. The stress-strain diagram I was trying to curve-fit is specimen no.3 shown in Fig. 36.

However, the analysis is non-linear and requires additional substeps as it demands convergence of the iterative solution procedure. The substeps are then representing increments of load within the single step at which the solution is carried out. Inside each individual substep, an iteration is performed that eventually arrives at the converged solution [93]. The convergence of the solution is attained by the Newton-Raphson method.

After running a few analyses (Fig. 50) and still receiving unsatisfactory results, I decided to split the analysis into 3 phases. During the first one, I specified a lower number of substeps and tried to curve-fit the tensile test as much as possible, saving some computation time due to the lower precision of the solution. During the second phase, I increased the number of substeps and proceeded to refine the process and material characteristics. During the third phase, I only performed three computations with a very high number of substeps to smoothen the curve and get an even better solution with little manipulation of the material properties.
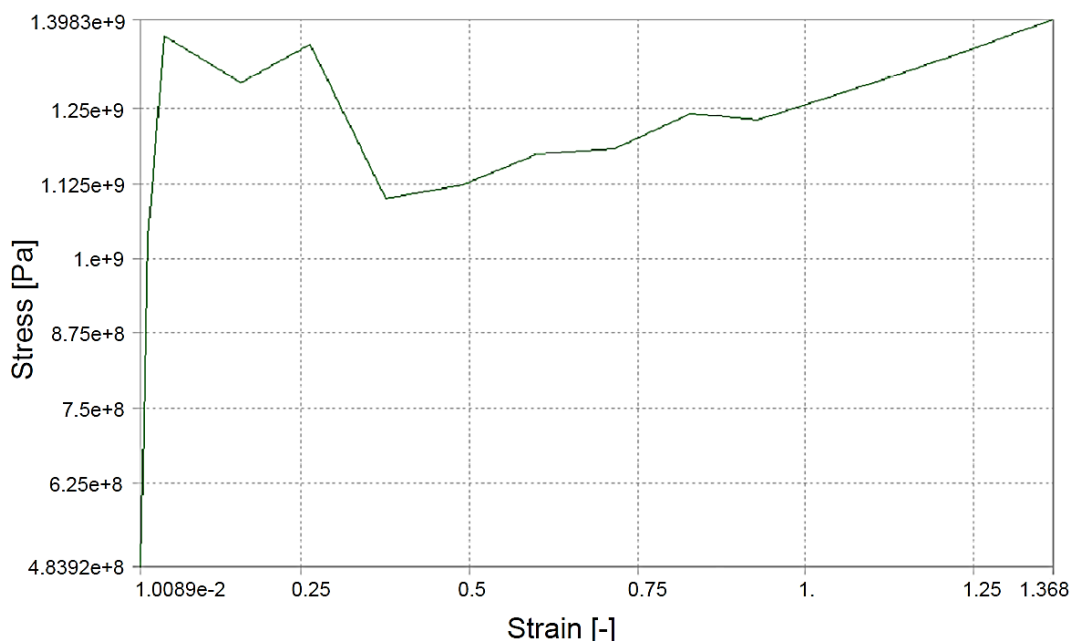
Fig. 50: One of the first stress-strain diagrams obtained before considering the precision of the solution. Also computed with no knowledge of proper material properties values.

The number of substeps for the first (estimating) phase was set to a minimum of 50 and a maximum of 100 substeps inside a 42 seconds long load interval (step). The program then automatically handled the required amount of substeps based on the convergence of the

problem. The computation time of this particular solution was around 25 minutes and was performed approximately 25 times. Below is shown the convergence of the solution (Fig. 51) as well as one of the stress-strain diagrams of the estimating phase (Fig. 52).
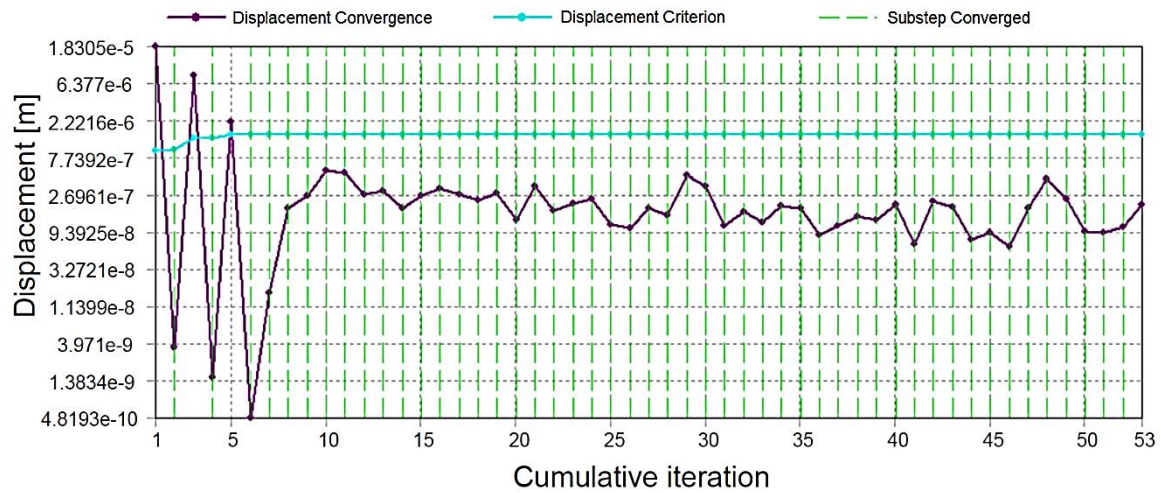
Fig. 51: The convergence criterion across all iterations of the first (estimating) phase. An iteration is computed in each substep of the solution.
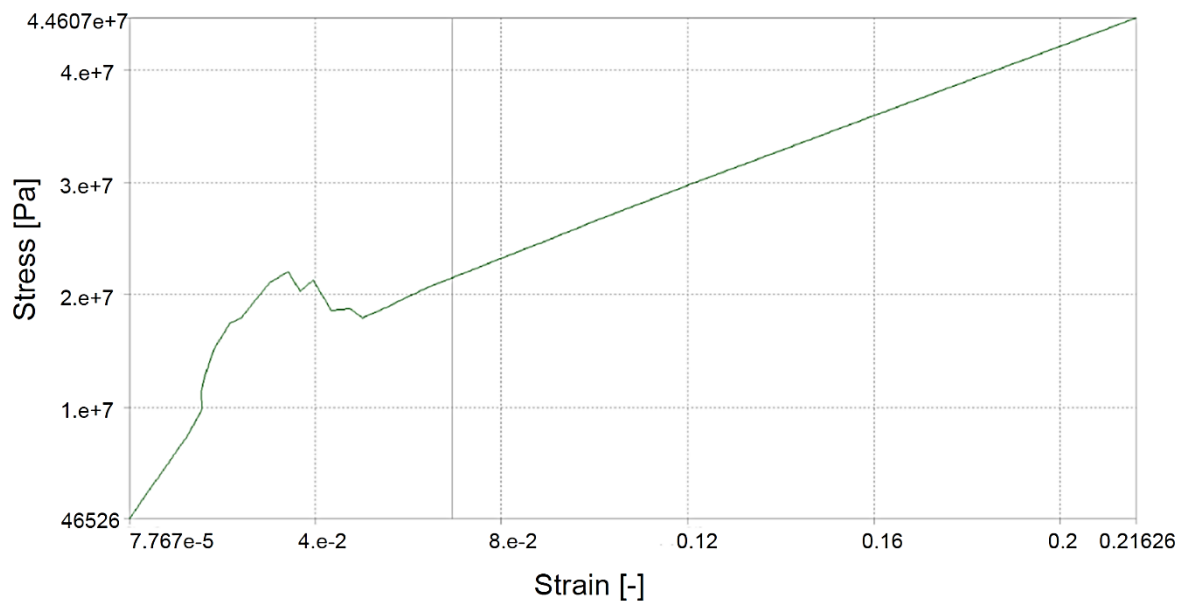
Fig. 52: The stress-strain diagram obtained from the last solution of the first (estimating) phase of the curve-fitting process. At this point, material properties are closer to the desired values presented in Fig. 49.

The subsequently performed refining phase then contained a minimum of 100 and a maximum of 200 substeps. The solution convergence was not affected (as the solution was already well-converged with less substeps, as shown in Fig. 51), but I observed a positive change in the curve-fitting process, so I proceeded to add more substeps in the analysis so as to obtain a better-shaped curve. During this process, I was also further manipulating the

material properties of the model. The results of the second (refining) phase of the curve-fitting process are shown in Fig. 53 and Fig. 54. The two main properties I was changing throughout the whole process were the values of Young's modulus E (the slope of the curve up until the range of yield strength) and tangent modulus E_t. Tangent modulus is a material property provided for non-linear analyses. It represents the slope of the curve in the range between the yield and ultimate strength. Other stable values, like yield strength, were manipulated only rarely throughout the curve-fitting process. The computation time of the second (refining) phase was around 40 minutes and was performed approximately 8 times.
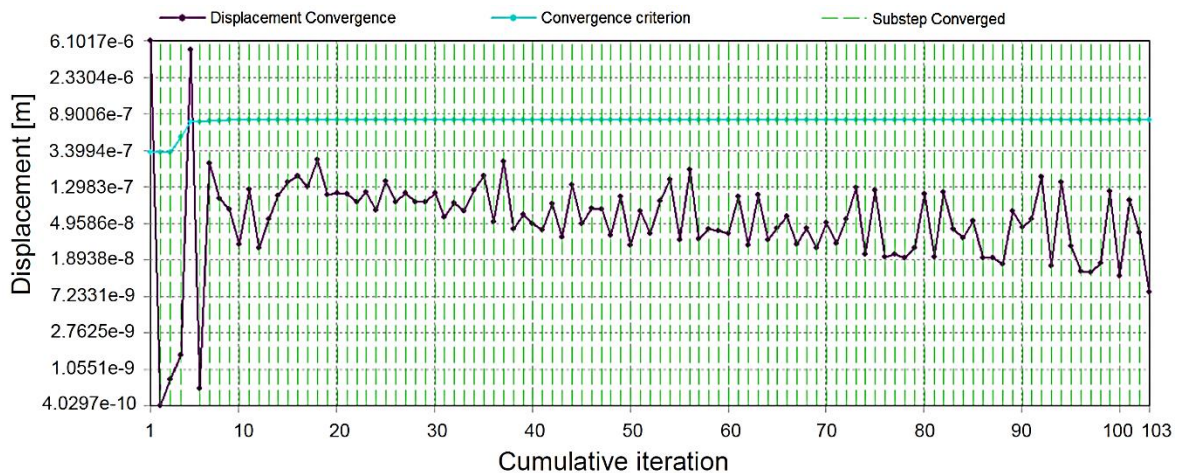
Fig. 53: The convergence criterion across all iterations of the second (refining) phase.
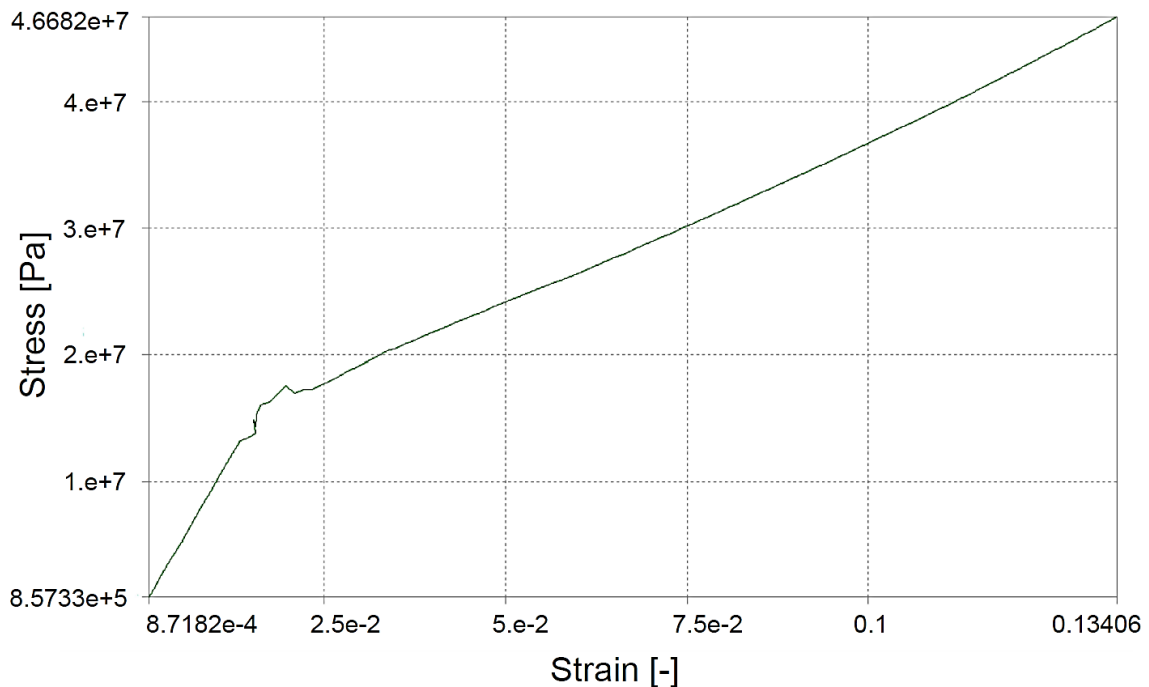
Fig. 54: The stress-strain diagram obtained from the last solution of the second phase of the curve-fitting process. Aside from the erratic region of yield strength, values of stress and their respective strain nearly correspond, although some adjustments are still necessary.

At the end of the second phase of the analysis, the values of stress and corresponding strain were already nearly satisfactory. I decided to enter the third and final phase of curve-fitting. In this phase, I specified a minimum of 300 and a maximum of 500 substeps. The computation time of this last solution was 2 hours and 6 minutes and it was performed only three times. Since the convergence of the problem was attained and no longer relevant, I left the corresponding graph out for the sake of brevity. The very final solution is shown in Fig. 55. The comparison of the experimental data and the final solution is shown in Fig. 56.
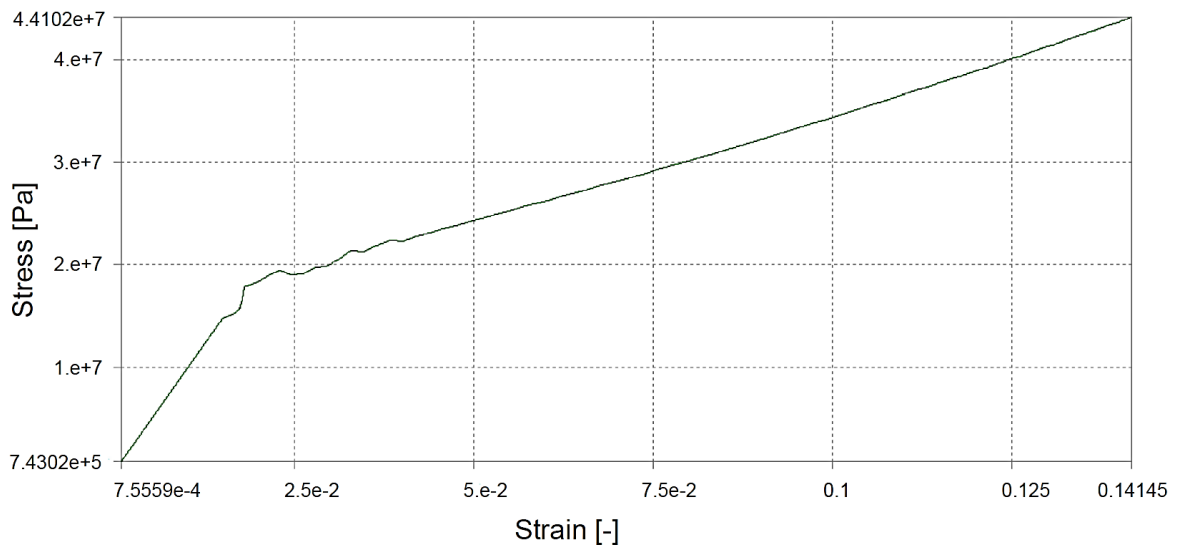
Fig. 55: The stress-strain diagram obtained from the last solution of the third (last) phase of the curve-fitting process. The curve is similar to that from the second phase, but the region of yield strength is different due to the larger number of substeps.
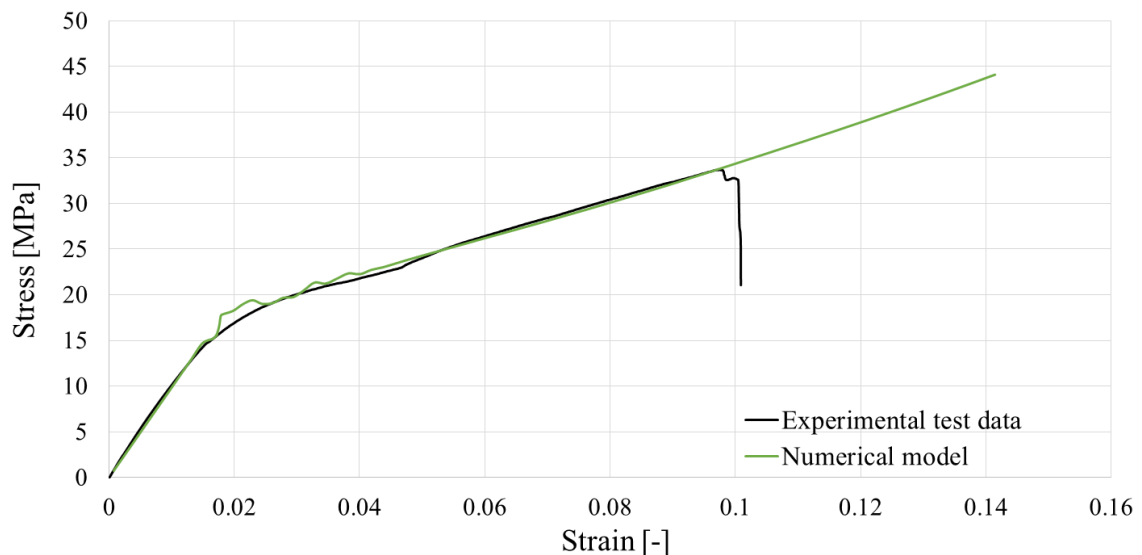
Fig. 56: The final curve containing the final material properties (green) in comparison with the experimental test data (black). The complete result of the curve-fitting process. The region of yield strength is still a little erratic, which is a feature that cannot seem to be eliminated. Corresponding material properties listed in Fig. 49.

7.7 Future prospects

It was anticipated that a complete analysis of the trabecular structure would be beyond the limits of a single thesis. Thus, in this chapter, I will address further problems that have arisen during the mechanical and numerical analyses and there was not enough space to consider them in this work. Also, I will mention other approaches that are not necessarily problems, but rather continuous, related efforts that will be examined in the future.

The first, very obvious problem that needs to be explained is the unattained failure of the model. This is true due to the fact that the Ansys Workbench software is unable to provide solution including the failure of the model without using special methods. The approach towards the failure of the model can be twofold – either by implementing additional APDL commands or using the xFEM fracture mechanics. After consulting with specialists from SVS FEM, s. r. o., I have determined that the more suitable approach will be to implement the APDL commands into the solver. The special commands needed to implement are called the *ekill/ealive algorithms*. They were not implemented in this thesis because of the already great volume of data that needed to be computed and processed.

The *ekill/ealive algorithms* can ensure that the model will fail upon reaching certain pre-defined limits. In the case of this problem, the limits can be specified either as maximum stress or maximum strain. When a mesh element reaches these limits, the solver will attribute its value in the stiffness matrix with a reduction coefficient (typically 10^{-6}, or however the user specifies it) that virtually discards it from the elements mesh, thus preventing the material from hardening beyond the specified limits to infinity [94]. This process is referred to either as the *birth* or the *death* of an element (but rather than really „killing" the element, it simply has its stiffness reduced while still being present in the solution and mesh). This process is checked and repeated after every iteration (step) of the solution, therefore I expect the computation times to increase even further.

Implementing these algorithms will be the next effort in the approach towards modeling and describing the mechanical behavior of the trabecular structure together with creating a finer mesh. The computational demands will show whether a special cluster computer will be needed or a regular multi-core processor PC will suffice.

After the model has been improved, the next major step will be to apply it onto a real implant. That can be considered the major focus of the whole effort. Before I delve further

into the specific application, I would like to mention two novel types of implants that have been invented and patented. These implants have been developed within the same project as my research and experiments. The implants have been invented and patented in Czech Republic and are shown in the figures below. On the basis of the patent application PV 2014-795, the patent n.306457 has been granted for the „four clover" implant variant (Fig. 57 a) and on the basis of the patent application PV 2014-794, the patent n.306456 has been granted for the „ribbed" implant variant by authors F. Denk Jr., A. Jíra and F. Denk Sr.

a) the „four leaf clover" implant variant, comprising of a cylindrical body and four rounded grooves encompassed in a hemisphere, forming a firm anchoring that ensures vertical and torsional stability

b)   the   „ribbed"   implant   variant, comprising of a cylindrical upper body part continuing with a conical system of four beams (ribs) and ending with a through transversal opening

Fig. 57: Two types of novel implants that have been developed in Czech Republic by authors F. Denk Jr., A. Jíra and F. Denk Sr. and subsequently patented. Implant type b) and its other variants were previously mentioned in Fig. 21.

The aforementioned novel implant types were introduced because the variant shown in Fig. 57 a), the „four leaf clover", will be the implant used for further applications of the numerical model. The variant shown above is a conventionally machined implant, but my further effort will be to create a model that will combine both the homogeneous and trabecular structure. This will be done by combining a homogeneous, machined stem with a trabecular, 3D-printed outer shell. The benefits and challenges of combining materials with different moduli has already been mentioned in chapter 5.2 Osseointegration and low modulus.

.

This conjunction will ultimately be the purpose of the model as a detailed analysis will be needed to determine the stress distribution and character of failure of an implant that combines multiple materials. The approach towards the model will be twofold, as mentioned in chapter 7.1 Purpose of the model and its introduction. The alternative of applying the experimentally determined properties of the virtual material to a homogeneous structure is considered a second, less appealing option, as the character of deformation, failure character of the outer layer and stress distribution is undetectable.

The main goal will be to create a model consisting of both the homogeneous and trabecular structure. That way it is possible to observe the full mechanical behavior of the morphologically complex structure as it truly represents the real implant. I already have at my disposal the STL files needed to create the model and merge the two materials together (Fig. 58 a) and Fig. 58 b))
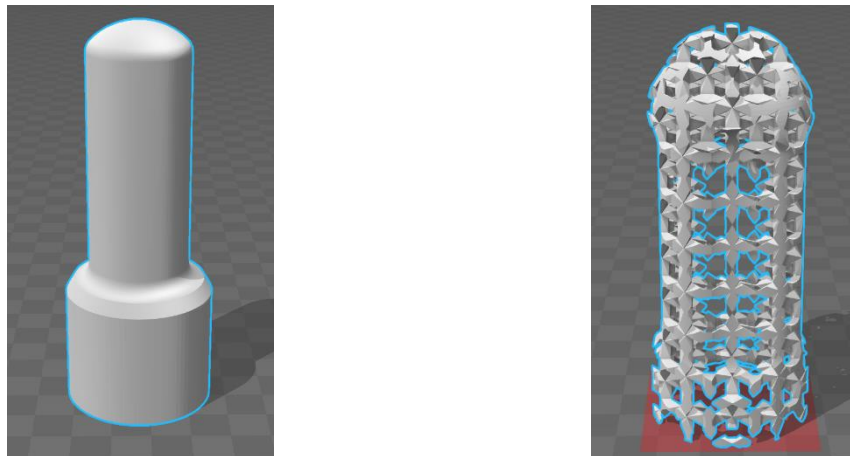
a) the STL model of the homogeneous stem   b) the STL model of the trabecular outer layer that represents the „four leaf clover"

Fig. 58: The STL geometries that will be merged together in a single implant model and used to create a combined implant variant of the „four leaf clover" implant type. Please refer to Fig. 24 for the geometry of the merged model.

With the virtual material properties curve-fitted, the next step will be to create this model and apply the material properties to the trabecular portion of the implant. It is expected that the trabecular portion will need a finer mesh compared to the homogeneous stem as the geometry is complex and contains thin beams. This process might prove to be demanding in regard to duration of the computation and it is expected that a special computer might be needed to perform this analysis.

8 Conclusion

The novel trabecular structure has been discussed, experimentally tested and had its experimental tensile test data curve-fitted by means of numerical modeling in the FEM software Ansys Workbench. The conducted tests were nanoindentation, global mechanical tests and in-vivo tests.

Production of the specimens was performed by 3D printing. The 3D printing technology is the only available method of manufacturing morphologically complex structures and brings many benefits but also some inconveniences. One of the obvious benefits is the ability to create complex structures or a quick manufacturing process that does not require large batches of specific products to be created, as opposed to machining. However, the major disadvantage is the quality of the final product. It was found that the beams of the 3D-printed structures vary in width and sometimes even disconnect, especially at the interface of the trabecular and homogeneous portions (Fig. 28 and Fig. 29). This production issue is limiting the ability to fully implement the structure in an automated production process as the occurrences seem to be completely random and visual control of every created product is needed. This negative feature, however, should be attributed to the novel technology that is not optimized for this particular task yet. I expect it to be overcome in time.

The potential biomechanical benefits of the structure are still to be proven true or false as there is not enough data and no documented history of success rates. The resemblance to the actual human bone structure is very promising and allows for both bone ongrowth and ingrowth, as opposed to homogeneous implants which only allow the bone to grow on the surface of the implant. Conducted in-vivo tests on pigs show that the living tissue is able to grow inside the trabecular structure and form new beams of bone directly in contact with the beams of the trabecular structure (Fig. 38). However, full osseointegration was not achieved. The percentage of bone-implant contact after 6 months following implantation is, however, still worse when compared to conventional homogeneous implants. My opinion is that more tests will definitely be needed as a single in-vivo test cannot provide a dependable result and

the trabecular structure might even need slightly different techniques of implantation and healing periods.

Nanoindentation tests have proven that the 3D-printed material can be fully compared to conventionally created structures as the material properties given by the manufacturer of the metal powder correspond with the properties obtained on the micro level. The micromechanical analysis has also proven the values of properties to be dependent on the depth of the indent (or the size of the loading force; please refer to Tab. 6). From a contact depth of $H_c \sim 470$ nm (corresponding force of 20 mN), the trend of E_r and H_{it} is constant. We can therefore assume the loading force of 20 mN as a basic value. The corresponding properties of this force are reduced modulus $E_r = 118$ GPa and hardness $H_{it} = 5.187$ GPa.

The global mechanical tests were conducted as a pilot experiment and cannot, therefore, be compared with other authors. As expected, by incorporating the trabecular structure, the values of modulus E were significantly reduced (Tab. 7). I did not know how much would the modulus be reduced and, to my surprise, I found out that the modulus was reduced over a 100 times. The tensile test has shown that the material has a bilinear stress-strain diagram with isotropic hardening (Fig. 36). The nature of deformation in the compression test was rather erratic, which is a fact that can be attributed to individual layers of the trabecular structure locking into one another while collapsing. This deformation is completely random, probably based on individual imperfections and local losses of stability. While the individual layers interlock, one can observe significant compression hardening before the collapse of another layer (Fig. 37).

Tab. 9: Final overview of different dental materials and test specimen and their moduli E and E_r. Comparison of conventional materials, values from experiment and human tissue.

	[1]Conventional Ti-6Al-4V [51]	[2]Rematitan powder (Dentaurum)	[2]Nanoindentation test (trab.)	[1]Tensile test (trab.)	[1]Compression test (trab.)	[2]Human bone [87]*
Mean E^1 or E_r^2 [GPa]	112.000	115.000	120.000	0.974	0.960	25.000

*Values can vary significantly based on bone density and overall health of individuals.

With the experimental tensile test data as a baseline, I performed the curve-fitting process. After several attempts to provide a solution with the default, large model used for 3D-printing, I decided to create a smaller model instead (Fig. 41). This reduction has proven to be a good decision since the academic license would not have allowed me to mesh the

model properly as it is limited by the maximum number of nodes in the mesh. Another great benefit of this reduction was the improvement of computation times, which needed to be taken into consideration, since there were many trial and error-type procedures and many computation errors in modeling such an atypic structure.

Curve-fitting has been done in three phases with increasing precision of the solution. After approximately 30 solutions, the desired shape of the curve has been successfully attained with the exception of model failure beyond the limits of ultimate stress or elongation at fracture (Fig. 56). This fact is fully acknowledged, addressed in chapter 7.7 Future prospects and will be improved upon by incorporating the *ekill/ealive algorithms* in future efforts.

With the curve-fitted material properties at hand (Fig. 49), the next task will be to apply these properties onto an implant incorporating both the trabecular and homogeneous structures and observe its mechanical behavior. The analysis of this merged implant (Fig. 58) will be one of the final goals of this research.

9 List of Figures

10 List of Tables

11 References

[1] Aguirre, A., 2002. Ancient esthetic dentistry in Mesoamerica. *Alpha Omegan*, *95*(4), p.21.

[2] Abraham, C.M., 2014. Suppl 1: A Brief Historical Perspective on Dental Implants, Their Surface Coatings and Treatments. The open dentistry journal, 8, p.50.

[3] Lloyd, C.H., Scrimgeour, S.N., Brown, D., Clarke, R.L., Curtis, R., Hatton, P.V., Ireland, A.J., McCabe, J.F., Nicholson, J., Sherriff, M. and Strang, R., 1995. Dental materials: 1993 literature review. *Journal of dentistry*, *23*(2), pp.67-93.

[4] Bencharit, S., Byrd, W.C., Altarawneh, S., Hosseini, B., Leong, A., Reside, G., Morelli, T. and Offenbacher, S., 2014. Development and Applications of Porous Tantalum Trabecular Metal-Enhanced Titanium Dental Implants. Clinical implant dentistry and related research, 16(6), pp.817-826.

[5] WebMD, (2016). *Dental Health and Dentures*. [online] Available at: http://www.webmd.com/oral-health/dental-health-dentures#1 [Accessed 23 Oct. 2016].

[6] Beachmere Dental, (2014). *Full and Partial Dentures*. [online] Available at: http://beachmeredental.com.au/full-and-partial-dentures/ [Accessed 23 Oct. 2016].

[7] American Academy of Implant Dentistry, (2013). Non-Implant Options. [online] Available at: http://www.aaid-implant.org/dental-implant-options/non-implant-options/ [Accessed 24 Oct. 2016].

[8] WebMD, (2016). *Dental Health and Bridges*. [online] Available at: http://www.webmd.com/oral-health/guide/dental-health-bridges#1 [Accessed 24 Oct. 2016].

[9] Infodentis, *Dental Bridges Advantages.* [online] Available at: http://www.infodentis.com/dental-bridge/dental-bridges-advantages.php [Accessed 24 Oct. 2016].

[10] Infodentis, *Dental Bridges Advantages.* [online] Available at: http://www.infodentis.com/dental-bridge/dental-bridges-advantages.php [Accessed 24 Oct. 2016].

[11] Smiles on Bristol Dentistry, (2016). *Dental Bridges*. [online] Available at: http://smilesonbristoldentistry.com/tag/dental-bridge/ [Accessed 25 Oct. 2016].

[12] Randow, K., Glantz, P.O. and Zöger, B.O., 1986. Technical failures and some related clinical complications in extensive fixed prosthodontics: an epidemiological study of long-term clinical quality. *Acta Odontologica Scandinavica*, *44*(4), pp.241-255.

[13] Colgate, (2016), *Four types of Dental Bridges*, [online] Available at: http://www.colgate.com/en/us/oc/oral-health/cosmetic-dentistry/bridges-and-crowns/article/four-types-of-dental-bridges-0616 [Accessed 26 Oct. 2016].

[14] Sunrise Family Dentistry, (2013), *Bridges*, [online] Available at: http://sunrisefamily dentistry.com/services-and-procedures/bridges/ [Accessed 28 Oct. 2016].

[15] Everything Dentistry, (2013), *Resin Bonded Bridges*, [online] Available at: https://everythingdentistry.wordpress.com/tag/dental-bridge/ [Accessed 28 Oct. 2016].

[16] Medicodent, (2016), *Historie Implantologie*, [online] Available at: http://www.medicodent.cz/nas-system/historie-implantologie/ [Accessed 30 Oct. 2016].

[17] Zuby, (2010), *I. Implantáty – úvod*, [online] Available at: http://www.zuby.cz/implantaty/i-implantaty-uvod.html#2 [Accessed 30 Oct. 2016].

[18] Criss Piessens Clinic, (2016), *Dental Implant History*, [online] Available at: http://www.crispiessensclinic.com/implant_history.html [Accessed 30 Oct. 2016].

[19] American Academy of Implant Dentistry, (2016), *About Dental Implants*, [online] Available at: http://www.aaid.com/about/Press_Room/History_and_Background.html [Accessed 2 Nov. 2016].

[20] Pocket Dentistry, (2015), *Pioneers and Milestones in the Filed of Orthodontics and Orthodontic Surgery*, [online] Available at: http://pocketdentistry.com/2-pioneers-and-milestones-in-the-field-of-orthodontics-and-orthognathic-surgery / [Accessed 3 Nov. 2016].

[21] Baker Street Dental Group, (2012), [online] Available at: http://www.bakerstreetdental.com/news/wp-content/uploads/2012/05/5046647_blog.jpg [Accessed 3 Nov. 2016].

[22] Sullivan, R.M., 2001. Implant dentistry and the concept of osseointegration: a historical perspective. *J Calif Dent Assoc*, 29(11), pp.737-45.

[23] Mano Implantai, (2014), *History of Dental Implants*, [online] Available at: http://www.manoimplantai.lt/dantu-implantai/dantu-implantu-istorija/?lang=en [Accessed 3 Nov. 2016].

[24] Medicinenet, (2016), *Definition of Allograft*, [online] Available at: http://www.medicinenet.com/script/main/art.asp?articlekey=30941 [Accessed 5 Nov. 2016].

[25] Linkow, L.I. and Dorfman, J.D., 1990. Implantology in dentistry. A brief historical perspective. *The New York state dental journal*, 57(6), pp.31-35.

[26] Linkow, L.I. and Chercheve, R., 1970. *Theories and techniques of oral implantology* (Vol. 1). CV Mosby Co.

[27] Goldberg, N.I. and Gershkoff, A., 1949. The implant lower denture. *Dental digest*, *55*(11), pp.490-494.

[28] Linkow, L.I. and Dorfman, J.D., 1990. Implantology in dentistry. A brief historical perspective. *The New York state dental journal*, *57*(6), pp.31-35.

[29] Dentaledu, (2016), *Different Types of Dental Implants to choose from*, [online] Available at: http://www.dentaledu.tv/types-of-implants/ [Accessed 5 Nov. 2016].

[30] Jemt, T., 1991. Failures and Complications in 391 Consecutively Inserted Fixed Prostheses Supported by Brånemark Implants in Edentulous Jaws: A Study of Treatment From the Time of Prosthesis Placement to the First Annual Checkup. *International Journal of Oral & Maxillofacial Implants*, *6*(3).

[31] Gaviria, L., Salcido, J.P., Guda, T. and Ong, J.L., 2014. Current trends in dental implants. *Journal of the Korean Association of Oral and Maxillofacial Surgeons*, *40*(2), pp.50-60.

[32] UCONN Health, (2014), *Dental Implants: Are They for Me?*, [online] Available at: http://dentalimplants.uchc.edu/about/surgery_osseointegration.html [Accessed 5 Nov. 2016].

[33] Nobel Biocare, (2016), *History – Nobel Biocare*, [online] Available at: https://www.nobelbiocare.com/ie/en/home/company/about-us/history.html?redirect=true [Accessed 5 Nov. 2016].

[34] BioHorizons, (2015), *Tapered Internal Implant System*, [online] Available at: http://www.biohorizons.com/taperedinternal.aspx [Accessed 5 Nov. 2016].

[35] Harrell Dental Implant Center, (2015), *All-on-4 Dental Implants*, [online] Available at: http://harrelldentalimplantcenter.com/all-on-4-charlotte-nc/ [Accessed 5 Nov. 2016].

[36] Surgery Encyclopedia, (2016), *Dental Implants*, [online] Available at: http://www.surgeryencyclopedia.com/Ce-Fi/Dental-Implants.html [Accessed 8 Nov. 2016]

[37] Dentaledu, (2016), *Complete Dental Implant Cost Guide*, [online] Available at: http://www.dentaledu.tv/ [Accessed 5 Nov. 2016].

[38] Cowin, S.C. and Hegedus, D.H., 1976. Bone remodeling I: theory of adaptive elasticity. *Journal of Elasticity*, *6*(3), pp.313-326.

[39] Colgate, (2013), *Single Tooth Implants*, [online] Available at: http://www.colgate.com /en/us/oc/oral-health/cosmetic-dentistry/implants/article/single-tooth-implants [Accessed 5 Nov. 2016].

[40] 1888 Implant, (2012), *Dental Implant Types*, [online] Available at: http:// www.1888implant.com/mobile/dental_implants.html [Accessed 7 Nov. 2016].

[41] Dental Implant Group, (2016), *Ramus Frame Implants*, [online] Available at: http:// www.dentalimplantgroup.co.uk/ramus-frame-implants/#.WDWU5PnhBPY [Accessed 7 Nov. 2016].

[42] Facialart, (2016), [online] Available at: https://www.facialart.com/wp-content/gallery/bridge-or-implant/ [Accessed 7 Nov. 2016].

[43] Binon, P.P., 2000. Implants and components: entering the new millennium. *The International journal of oral & maxillofacial implants*, *15*(1), p.76.

[44] Saini, M., Singh, Y., Arora, P., Arora, V. and Jain, K., 2015. Implant biomaterials: A comprehensive review. *World Journal of Clinical Cases: WJCC*, *3*(1), p.52.

[45] Dental Implant USA, (2016), *What are Metal-free Dental Implants?*, [online] Available at: https://www.dentalimplantsusa.com/zirconium-metal-free-dental-implants.php [Accessed 9 Nov. 2016].

[46] Vancouver Centre for Cosmetic & Implant Dentistry, (2016), *Types of Dental Implant Materials – Titanium vs Zirconia*, [online] Available at: http://www.vccid.com/types-of-dental-implant-materials-titanium-vs-zirconia/ [Accessed 9 Nov. 2016].

[47] Andreiotelli, M. and Kohal, R.J., 2009. Fracture strength of zirconia implants after artificial aging. *Clinical implant dentistry and related research*, *11*(2), pp.158-166.

[48] Özkurt, Z. and Kazazoglu, E., 2011. Zirconia dental implants: a literature review. *Journal of Oral Implantology*, *37*(3), pp.367-376.

[49] Depprich, R., Zipprich, H., Ommerborn, M., Naujoks, C., Wiesmann, H.P., Kiattavorncharoen, S., Lauer, H.C., Meyer, U., Kübler, N.R. and Handschel, J., 2008. Osseointegration of zirconia implants compared with titanium: an in vivo study. *Head & face medicine*, *4*(1), p.1.

[50] Bania, P.J., 1994. Beta titanium alloys and their role in the titanium industry. *Jom*, *46*(7), pp.16-19.

[51] Niinomi, M., 1998. Mechanical properties of biomedical titanium alloys. *Materials Science and Engineering: A*, *243*(1), pp.231-236.

[52] Geetha, M., Singh, A.K., Asokamani, R. and Gogia, A.K., 2009. Ti based biomaterials, the ultimate choice for orthopaedic implants–a review. *Progress in Materials science*, *54*(3), pp.397-425.

[53] Pics Hype, (2016), *Dental Abutment*, [online] Available at: http://picshype.com/dental-abutment [Accessed 13 Nov. 2016].

[54] Joseph, S. S., Froes, F. H., (1988). *Light Metal Age*, pp. 4-6.

[55] Froes, F. H., (2004), Titanium Alloys. In: J. K. Wessel, ed., *Handbook of Advanced Materials: Enabling New Designs*, [online] Available at: http://onlinelibrary.wiley.com/book/10.1002/0471465186 [Accessed 13 Nov. 2016].

[56] Kolli, R.P., Joost, W.J. and Ankem, S., 2015. Phase stability and stress-induced transformations in beta titanium alloys. *JOM*, *67*(6), pp.1273-1280.

[57] Arcam, (2016), *Ti6Al4V Titanium Alloy*, [online] Available at: http://www.arcam.com/wp-content/uploads/Arcam-Ti6Al4V-Titanium-Alloy.pdf [Accessed 18 Nov. 2016].

[58] Andrade, A., Morcelli, A. and Lobo, R., 2010. Deformation and fracture of an alpha/beta titanium alloy. *Matéria (Rio de Janeiro)*, *15*(2), pp.364-370.

[59] ASTM, F., 1995. F 67-95: Standard specification for unalloyed titanium for surgical implant application. *American Society for testing and materials, Philadelphia*.

[60] MTM, F., 1992. 136-92: Standard specification for wrought Ti-6A1-4V ELI alloy for surgical implant applications. *Annual Book of ASTM Standards. Philadelphia, PA, American Society for Testing and Materials*.

[61] ASTM, F., 1993. 1472-93: Standard specification for wrought Ti-6A1-4V alloy for surgical implant applications. *Annual Book of ASTM Standards. Philadelphia, PA, American Society for Testing and Materials*.

[62] Wataha, J.C., 1996. Materials for endosseous dental implants. *Journal of oral rehabilitation*, *23*(2), pp.79-90.

[63] Eisenbarth, E., Velten, D., Müller, M., Thull, R. and Breme, J., 2004. Biocompatibility of β-stabilizing elements of titanium alloys. *Biomaterials*, *25*(26), pp.5705-5713.

[64] Niinomi, M., 2008. Mechanical biocompatibilities of titanium alloys for biomedical applications. *Journal of the mechanical behavior of biomedical materials*, *1*(1), pp.30-42.

[65] Mei, S., Wang, H., Wang, W., Tong, L., Pan, H., Ruan, C., Ma, Q., Liu, M., Yang, H., Zhang, L. and Cheng, Y., 2014. Antibacterial effects and biocompatibility of titanium surfaces with graded silver incorporation in titania nanotubes. *Biomaterials*, *35*(14), pp.4255-4265.

[66] Niinomi, M., 2002. Recent metallic materials for biomedical applications. *Metallurgical and materials transactions A*, *33*(3), pp.477-486.

[67] da Silva, L.M., Claro, A.P.R.A., Donato, T.A.G., Arana-Chavez, V.E., Moraes, J.C.S., Buzalaf, M.A.R. and Grandini, C.R., 2011. Influence of Heat Treatment and Oxygen Doping on the Mechanical Properties and Biocompatibility of Titanium-Niobium Binary Alloys. *Artificial organs*, *35*(5), pp.516-521.

[68] Okazaki, Y., Ito, Y., Kyo, K. and Tateishi, T., 1996. Corrosion resistance and corrosion fatigue strength of new titanium alloys for medical implants without V and Al. *Materials Science and Engineering: A*, *213*(1), pp.138-147.

[69] Nag, S., Banerjee, R. and Fraser, H.L., 2005. Microstructural evolution and strengthening mechanisms in Ti–Nb–Zr–Ta, Ti–Mo–Zr–Fe and Ti–15Mo biocompatible alloys. *Materials Science and Engineering: C*, *25*(3), pp.357-362.

[70] Matsuno, H., Yokoyama, A., Watari, F., Uo, M. and Kawasaki, T., 2001. Biocompatibility and osteogenesis of refractory metal implants, titanium, hafnium, niobium, tantalum and rhenium. *Biomaterials*, *22*(11), pp.1253-1262.

[71] Gepreel, M.A.H. and Niinomi, M., 2013. Biocompatibility of Ti-alloys for long-term implantation. *Journal of the mechanical behavior of biomedical materials*, *20*, pp.407-415.

[72] Peden, M., 2004. World report on road traffic injury prevention.

[73] Köster, R., Vieluf, D., Kiehn, M., Sommerauer, M., Kähler, J., Baldus, S., Meinertz, T. and Hamm, C.W., 2000. Nickel and molybdenum contact allergies in patients with coronary in-stent restenosis. *The Lancet*, *356*(9245), pp.1895-1897.

[74] Boyce, B.F., Byars, J., McWilliams, S., Mocan, M.Z., Elder, H.Y., Boyle, I.T. and Junor, B.J., 1992. Histological and electron microprobe studies of mineralisation in aluminium-related osteomalacia. *Journal of clinical pathology*, *45*(6), pp.502-508.

[75] Hoseini, M., Bocher, P., Shahryari, A., Azari, F., Szpunar, J.A. and Vali, H., 2014. On the importance of crystallographic texture in the biocompatibility of titanium based substrate. *Journal of Biomedical Materials Research Part A*, *102*(10), pp.3631-3638.

[76] Le Guéhennec, L., Soueidan, A., Layrolle, P. and Amouriq, Y., 2007. Surface treatments of titanium dental implants for rapid osseointegration. *Dental materials*, *23*(7), pp.844-854.

[77] Cochran, D.L., Schenk, R.K., Lussi, A., Higginbottom, F.L. and Buser, D., 1998. Bone response to unloaded and loaded titanium implants with a sandblasted and acid-etched

surface: a histometric study in the canine mandible. *Journal of biomedical materials research*, *40*(1), pp.1-11.

[78] Wennerberg, A., Hallgren, C., Johansson, C. and Danelli, S., 1998. A histomorphometric evaluation of screw-shaped implants each prepared with two surface roughnesses. *Clinical oral implants research*, *9*(1), pp.11-19.

[79] Buser, D., Schenk, R.K., Steinemann, S., Fiorellini, J.P., Fox, C.H. and Stich, H., 1991. Influence of surface characteristics on bone integration of titanium implants. A histomorphometric study in miniature pigs. *Journal of biomedical materials research*, *25*(7), pp.889-902.

[80] Gotfredson, K., Wennerberg, A., Johansson, C., Skovgaard, L.T. and Hjørting-Hansen, E., 1995. Anchorage of TiO2-blasted, HA-coated, and machined implants: An experimental study with rabbits. *Journal of biomedical materials research*, *29*(10), pp.1223-1231.

[81] Wennerberg, A., Albrektsson, T., Andersson, B. and Krol, J.J., 1995. A histomorghometric study of screw-shaped and removal torque titanium implants with three different surface topographies. *Clinical oral implants research*, *6*(1), pp.24-30.

[82] Becker, W., Becker, B.E., Ricci, A., Bahat, O., Rosenberg, E., Rose, L.F., Handelsman, M. and Israelson, H., 2000. A Prospective Multicenter Clinical Trial Comparing One- and Two-Stage Titanium Screw-Shaped Fixtures with One-Stage Plasma-Sprayed Solid-Screw Fixtures. *Clinical implant dentistry and related research*, *2*(3), pp.159-165.

[83] Borah, B., Gross, G.J., Dufresne, T.E., Smith, T.S., Cockman, M.D., Chmielewski, P.A., Lundy, M.W., Hartke, J.R. and Sod, E.W., 2001. Three-dimensional microimaging (MRμI and μCT), finite element modeling, and rapid prototyping provide unique insights into bone architecture in osteoporosis. *The anatomical record*, *265*(2), pp.101-110.

[84] Wiria, F.E., Shyan, J.Y.M., Lim, P.N., Wen, F.G.C., Yeo, J.F. and Cao, T., 2010. Printing of titanium implant prototype. *Materials & Design*, *31*, pp.S101-S105.

[85] El-Hajje, A., Kolos, E.C., Wang, J.K., Maleksaeedi, S., He, Z., Wiria, F.E., Choong, C. and Ruys, A.J., 2014. Physical and mechanical characterisation of 3D-printed porous titanium for biomedical applications. *Journal of Materials Science: Materials in Medicine*, *25*(11), pp.2471-2480.

[86] Dabrowski, B., Swieszkowski, W., Godlinski, D. and Kurzydlowski, K.J., 2010. Highly porous titanium scaffolds for orthopaedic applications. *Journal of Biomedical Materials Research Part B: Applied Biomaterials*, *95*(1), pp.53-61.

[87] Řehounek, L. 2015, Experimental micromechanical analysis of the tooth dentin, Bachelor's thesis, Czech Technical University in Prague, Prague.

[88] ABR Therapy, (2016), *Stress Shielding*, [online] Available at: http://abr-denmark.com /home/abr-therapy/why-abr/stress-shielding/ [Accessed 20 Nov. 2016].

[89] Sumner, D.R., 2015. Long-term implant fixation and stress-shielding in total hip replacement. *Journal of biomechanics*, *48*(5), pp.797-800.

[90] Hartmann-H'Lawatscheck, T., 2015. Metal Laser Melting. *Laser Technik Journal*, *12*(5), pp.41-43.

[91] Kubíková, T., Králíčková, M., Tonar, Z. (2016). *Histologické hodnocení oseointegrace implantátů podle ISO normy 10993-6*.

[92] Steinberg, D., 1996. *Equation of state and strength properties of selected materials* (pp. 3-6). Livermore, CA: Lawrence Livermore National Laboratory.

[93] Sharcnet, (2016), *Steps, Substeps, and Equilibrium Iterations*, [online] Available at: https://www.sharcnet.ca/Software/Ansys/17.0/en-us/help/wb_sim/ds_Steps_Substeps _Eq.html [Accessed 4 Jan. 2017].

[94] Sharcnet, (2016), *Performing a Nonlinear Static Analysis*, [online] Available at: https://www.sharcnet.ca/Software/Ansys/16.2.3/en-us/help/ans_str/Hlp_G_STR8_13 .html [Accessed 6 Jan. 2017].